816. Bearings coefficients effects on chaotic and bifurcation behavior of flexible rotor systems subjected to rub-impact

H. M. Khanlo[1], M. Ghayour[2], S. Ziaei-Rad[3]
[1]Department of Aerospace Engineering, Aeronautical University of Science and Technology
Tehran 13846-73411, Iran
[2, 3]Department of Mechanical Engineering, Isfahan University of Technology, Isfahan 84156-83111, Iran
E-mail: [1]*khanloh47@yahoo.com*, [2]*ghayour@cc.iut.ac.ir*, [3]*szrad@cc.iut.ac.ir*

(Received 2 May 2011; accepted 20 May 2012)

Abstract. This study investigates the influence of end-support conditions on the chaotic and bifurcation behavior of a rotating flexible shaft-disk system. The system is modeled as a continuous shaft with a rigid disk in its mid span whilst supported by multi-coefficients bearings. Both Coriolis and centrifugal effects due to shaft flexibility are included. The partial differential equations of motion are extracted using the Rayleigh beam theory and the assumed mode method is used to discretize them in order to be solved numerically. The analytical tools used in this work include time series, phase plane portrait, power spectrum, Poincaré map, bifurcation diagrams, and Lyapunov exponents. The main objective of the present study is to investigate the effects of end-supports stiffness and damping coefficients on the chaotic vibration behavior of a rotating system. Periodic, sub-harmonic, quasi-periodic, and chaotic states have been observed for each case. As demonstrated, inclusion of the bearing effects can primarily change the speed ratios at which rub-impact occurs. The principal and cross-coupling stiffness and damping coefficients have quite different effects in the chaotic behavior of the system.

Keywords: eight-coefficient bearings, dynamic behavior, chaotic, bifurcation, flexible shaft.

1. Introduction

Shafts or shaft-bearing assemblies are the most important components of rotating machinery. Study of shaft-bearing characteristics is a necessary step for the design of machine elements. The early rotor dynamic analysis show that designers knew about the large influence of shaft supports on the behavior of rotating machinery. Bearings were the first support components whose effects have been included in the analysis, followed by squeeze film dampers and other forms of bearings. The bearings play an important role in the dynamic response and stability of shaft-bearing systems where in many instances a bearing change, which is usually a minor modification, can improve the dynamic behavior of the system.

Increasing demands for efficient industrial production have placed stringent requirements on designers and developers to produce high speed, high performance and trouble-free rotating machinery. However, some troubles, such as rub-impact between rotor and stator, can occur during the operation of rotating machinery. Ignoring the occurrence of rubbing may lead to catastrophic failures of the rotating machinery, a fact which has implied the urge necessity of its consideration in the dynamic analysis.

Huang et al. [1] investigated the stability of elastic shaft-rigid disk bearing system by Lyapunov method. In their model, the end supports were modeled as eight-coefficient bearings, then various end support parameters were studied. Rao et al. [2] used an eight-coefficient bearing to finite element formulation of a geared rotor system. Marhomy [3] studied the stability of elastic shaft bearing systems with nonlinear bearing parameters. His numerical results showed that nonlinearity of bearing stiffness and damping parameters can influence the whirling stability of rotor-bearing systems. The vibration analysis of rotor shaft system with nonlinear bearing model is investigated by Ji et al. [4]. The rotating shaft is described by the Timoshenko beam

© VIBROENGINEERING. JOURNAL OF VIBROENGINEERING. JUNE 2012. VOLUME 14, ISSUE 2. ISSN 1392-8716

theory and the nonlinear bearings have cubic nonlinear stiffness and linear damping characteristics. The method of multiple scales was used for free and forced vibration analysis of the shaft-rotor system. Their results showed a jump corresponding to the multi-valued phenomenon and bifurcation character of the system. Marhomy et al. [5] studied the stability of rotor-bearing systems by Routh-Hurwitz criterion. The stability analysis has been performed on a rotor-bearing system modeled as an axially symmetric appendage at the mid-span of a spinning shaft mounted on two dissimilar eight-coefficient end-bearings. The results showed that the anisotropy of the bearing's damping coefficients is a source of whirl instability. Hu et al. [6] used a finite element-based formulation for modeling the dynamic behavior of a rotating flexible shaft supported by a flexible support structure. The supporting mechanism between the rotating flexible shaft and the flexible basis was represented by three sets of non-linear springs at each support location. Wu [7] investigated the prediction of lateral vibration of a full-size rotor-bearing system by using those of its scaled model. He used the eight-coefficient bearing for modeling the end supports in order to mathematically formulate the system. Ishida et al. [8] studied the nonlinear resonances and self-excited oscillations of a rotor caused by radial clearance and collision. In their model, the shaft was simply supported at both ends and the bearings were fixed in radial direction. An equivalent spring and damper model was introduced to simulate the collision in the clearance between the bearing and holder. Meruane et al. [9] considered up to third order terms on the Taylor expansion to model the stiffness and damping coefficients of the bearing fluid film reaction in terms of both perturbation displacements and velocities. Baguet et al [10] used the hydrodynamic journal bearing model for nonlinear dynamic analysis and eight-coefficient model for a linear dynamic analysis in the gear-shaft-bearing system.

Va´zquez et al. [11] presented an experimental study on the stability and unbalance response of a flexible rotor supported by fluid film bearings. Their results indicated that the support flexibility does not influence the first critical speed. In addition, the stability thresholds increased with the support flexibility. Lin [12] studied the dynamic characteristics and film instability of a rotor-bearing system lubricated with couple stress fluids. His results showed that the couple stresses provide an increase in the values of the stiffness coefficients as well as the damping characteristics. Legrand et al. [13] investigated the vibrational behavior of the rotating shaft supported by short nonlinear journal bearings at its two ends. They used a Rayleigh beam with uniform cross-section properties to model the shaft and Reynolds' equation to evaluate the oil film pressure distribution on the bearings. Chang-Jian et al. [14, 15] studied the nonlinear behavior of a flexible rotor supported by squeeze couple stress fluid film journal bearings. His results revealed that the couple stress fluid model is superior and more stable than the traditional Newtonian fluids. In addition, the couple stress fluid is shown to improve the dynamic behavior of the rotor-bearing system.

The squeeze-film dampers are commonly used in conjunction with rolling-elements or hydrodynamic bearings in rotating machinery. Some researchers such as [16, 17] studied the dynamic behavior of rotor-bearing systems with different models for end supports. Recently, researchers [18, 19] investigated the active control of rotor-bearing systems. The control action can be applied to either bearings or shaft. By applying these control actions, one may enhance the stability limit or restrain the disorder behavior of the system.

To the best of the authors' knowledge, no work has been reported on the influence of end-support conditions on the chaotic behavior of rotating continuous shafts-disk systems with rub-impact considered. In this work, a continuous flexible shaft with a rigid disk in the mid span and eight-coefficient bearing at the end-supports is considered. The assumed mode method is used to discretize the partial differential equations of motion, which leads to nonlinear coupled differential equations that are solved numerically. Accuracy of the solutions is shown not to improve substantially by including an unnecessary higher number of modes. Time series, phase plane portrait, power spectra, Poincaré map, bifurcation diagrams, and Lyapunov exponents are

© VIBROENGINEERING. JOURNAL OF VIBROENGINEERING. JUNE 2012. VOLUME 14, ISSUE 2. ISSN 1392-8716

employed to investigate the behavior of the system. The main objective of the present study is to investigate the effects of end-supports on the chaotic vibration behavior of a rotating system.

2. Mathematical Formulation

In this study, the uniform Rayleigh beam theory is used for the mathematical modeling of a rotating shaft. Investigations in the shaft-disk system behavior are performed according to the following assumptions:

(1) Shear deformation is neglected;

(2) Shaft cross-section and material properties along its length are uniform, i.e. $I_y = I_z = I_s$;

(3) Area moment inertia of the disk are the same in the two principal directions, i.e. $I_{yd} = I_{zd} = I_d$;

(4) Internal damping is negligible;

(5) Axial and torsional vibration is neglected;

(6) Static deflections are negligible compared to dynamic effects.

The Coriolis and centrifugal forces due to the shaft flexibility can affect the dynamic behavior of the system [20]. Thus, these forces are included in the analysis. Fig. 1 shows the schematic of the rotating flexible shaft-disk system that is supported at its ends by two dissimilar eight-coefficient bearings.

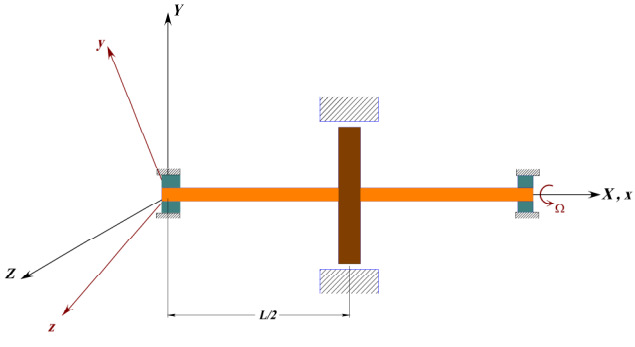

(a)

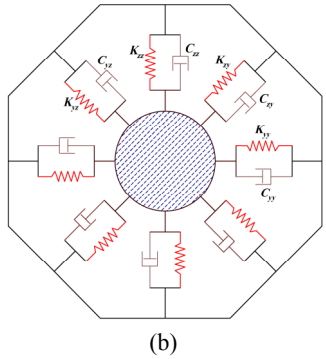

(b)

Fig. 1. Schematic diagram of (a) rotating flexible shaft-disk system (b) eight coefficient bearing

In the dynamic equilibrium configuration of the system, the undeformed shaft is the along the x direction of a rotating xyz coordinate frame. The left bearing deflection is denoted by $\mathbf{r}_1 = y_1\mathbf{j} + z_1\mathbf{k}$ and that of the right by $\mathbf{r}_2 = L\mathbf{i} + y_2\mathbf{j} + z_2\mathbf{k}$. The displacement of an arbitrary element of the shaft axis at a distance x from the left bearing in its undeformed configuration is described by [1]:

$$\mathbf{r}_u(x,t) = x\mathbf{i} + y(x,t)\mathbf{j} + z(x,t)\mathbf{k} = x\mathbf{i} + (y_1 + x\theta)\mathbf{j} + (z_1 + x\varphi)\mathbf{k} \tag{1}$$

where for small angles and displacements, these approximations become valid:

$$\theta = \frac{y_2 - y_1}{L}, \quad \varphi = \frac{z_2 - z_1}{L} \tag{2}$$

The shaft rotates about centerline of the bearings with angular velocity Ω. One can write the system's angular velocity in the body coordinates as:

$$\boldsymbol{\omega}_s = (\Omega + \theta\dot{\varphi})\mathbf{i} + (-\Omega\theta + \dot{\varphi})\mathbf{j} + (\Omega\varphi + \dot{\theta})\mathbf{k} \tag{3}$$

The angular velocity vector of the shaft element due to elastic displacements and bearing deflections in the body coordinate is:

$$\boldsymbol{\omega}_e = \begin{Bmatrix} \Omega + \theta\dot{\varphi} + \theta_e(-\Omega\theta + \dot{\varphi}) - \varphi_e(\Omega\varphi + \dot{\theta} + \dot{\theta}_e) \\ -\theta_e(\Omega + \theta\dot{\varphi}) - \Omega\theta + \dot{\varphi} + \dot{\varphi}_e \\ \varphi_e(\Omega + \theta\dot{\varphi}) + \Omega\varphi + \dot{\theta} + \dot{\theta}_e \end{Bmatrix} \tag{4}$$

where θ_e and φ_e are the local slopes of the flexible shaft element and are defined as:

$$\theta_e = \frac{\partial v(x,t)}{\partial x} = v'(x,t) \ , \ \varphi_e = -\frac{\partial w(x,t)}{\partial x} = -w'(x,t) \tag{5}$$

where the $\dot{(\ )}$ and $(\ )'$ denote differentiation with respect to time and displacement x, respectively.

The position vector of a typical differential shaft element at distance x along the shaft is:

$$\begin{aligned} \mathbf{r}_s(x,t) &= (y(x,t) + v(x,t))\mathbf{j} + (z(x,t) + w(x,t))\mathbf{k} \\ &= (y_1 + x\theta + v(x,t))\mathbf{j} + (z_1 + x\varphi + w(x,t))\mathbf{k} \end{aligned} \tag{6}$$

The velocity vector at the centerline of the shaft element is [21]:

$$\begin{aligned} \mathbf{v}_s(x,t) = &[(z_1 + x\varphi + w(x,t))(-\Omega\theta + \dot{\varphi}) - (y_1 + x\theta + v(x,t))(\Omega\varphi + \dot{\theta})]\mathbf{i} \\ &+ [(\dot{y}_1 + x\dot{\theta} + \dot{v}(x,t)) - (z_1 + x\varphi + w(x,t))(\Omega + \theta\dot{\varphi})]\mathbf{j} \\ &+ [(\dot{z}_1 + x\dot{\varphi} + \dot{w}(x,t)) + (y_1 + x\theta + v(x,t))(\Omega + \theta\dot{\varphi})]\mathbf{k} \end{aligned} \tag{7}$$

Suppose that the disk is mounted on the mid span of the shaft, $x = L/2$; hence, the angular velocity, position vector and velocity vector of the disk center are:

$$\boldsymbol{\omega}_d = \begin{Bmatrix} \Omega + \theta\dot{\varphi} + \theta_d(-\Omega\theta + \dot{\varphi}) - \varphi_d(\Omega\varphi + \dot{\theta} + \dot{\theta}_d) \\ -\theta_d(\Omega + \theta\dot{\varphi}) - \Omega\theta + \dot{\varphi} + \dot{\varphi}_d \\ \varphi_d(\Omega + \theta\dot{\varphi}) + \Omega\varphi + \dot{\theta} + \dot{\theta}_d \end{Bmatrix} \tag{8}$$

$$\mathbf{r}_d(L/2,t) = (y_1 + \frac{L}{2}\theta + v(L/2,t))\mathbf{j} + (z_1 + \frac{L}{2}\varphi + w(L/2,t))\mathbf{k} \tag{9}$$

$$\begin{aligned}\mathbf{v}_d(L/2,t) = {} & [(z_1 + \frac{L}{2}\varphi + w(L/2,t))(-\Omega\theta + \dot{\varphi}) - (y_1 + \frac{L}{2}\theta + v(L/2,t))(\Omega\varphi + \dot{\theta})]\mathbf{i} \\ & + [(\dot{y}_1 + \frac{L}{2}\dot{\theta} + \dot{v}(L/2,t)) - (z_1 + \frac{L}{2}\varphi + w(L/2,t))(\Omega + \theta\dot{\varphi})]\mathbf{j} \\ & + [(\dot{z}_1 + \frac{L}{2}\dot{\varphi} + \dot{w}(L/2,t)) + (y_1 + \frac{L}{2}\theta + v(L/2,t))(\Omega + \theta\dot{\varphi})]\mathbf{k}\end{aligned} \tag{10}$$

where θ_d and φ_d are the slopes of the rigid disk and are defined as:

$$\theta_d = \frac{\partial v(x,t)}{\partial x} = v'(x,t)\big|_{x=\frac{L}{2}},\ \varphi_d = -\frac{\partial w(x,t)}{\partial x} = -w'(x,t)\big|_{x=\frac{L}{2}} \tag{11}$$

The kinetic energy expression of the rotating shaft is:

$$\begin{aligned}T_s = {} & \frac{1}{2}\int_0^L \rho A(\mathbf{v}_s.\mathbf{v}_s)\,dx + \frac{1}{2}\int_0^L \rho(\boldsymbol{\omega}_s^{\mathrm{T}}\mathbf{I}\boldsymbol{\omega}_s)\,dx = \frac{1}{2}\int_0^L \Big\{\rho A\Big\{\Big[(z_1 + x\varphi + w(x,t))(-\Omega\theta + \dot{\varphi}) \\ & -(y_1 + x\theta + v(x,t))(\Omega\varphi + \dot{\theta})\Big]^2 + \Big[(\dot{y}_1 + x\dot{\theta} + \dot{v}(x,t)) - (z_1 + x\varphi + w(x,t))(\Omega + \theta\dot{\varphi})\Big]^2 \\ & + \Big[(\dot{z}_1 + x\dot{\varphi} + \dot{w}(x,t)) + (y_1 + x\theta + v(x,t))(\Omega + \theta\dot{\varphi})\Big]^2\Big\} + \rho\Big\{J_{ps}\Big[\Omega + \theta\dot{\varphi} \\ & + v'(x,t)(-\Omega\theta + \dot{\varphi}) + w'(x,t)(\Omega\varphi + \dot{\theta} + \dot{v}'(x,t))\Big]^2 + I_s\Big[-v'(x,t)(\Omega + \theta\dot{\varphi}) \\ & - \Omega\theta + \dot{\varphi} - \dot{w}'(x,t)\Big]^2 + I_s\Big[-w'(x,t)(\Omega + \theta\dot{\varphi}) + \Omega\varphi + \dot{\theta} + \dot{v}'(x,t)\Big]^2\Big\}\Big\}dx\end{aligned} \tag{12}$$

where ρ is shaft mass density, A is the cross-section area and I_s and J_{ps} are the diametral area moment of inertia and the polar area moment of inertia of the shaft, respectively.

The kinetic energy expression of a rigid disk is:

$$\begin{aligned}T_d = {} & \frac{1}{2}m_d\Big\{\Big[(z_1 + x\varphi + w(x,t))(-\Omega\theta + \dot{\varphi}) - (y_1 + x\theta + v(x,t))(\Omega\varphi + \dot{\theta})\Big]^2 \\ & + \Big[(\dot{y}_1 + x\dot{\theta} + \dot{v}(x,t)) - (z_1 + x\varphi + w(x,t))(\Omega + \theta\dot{\varphi})\Big]^2 \\ & + \Big[(\dot{z}_1 + x\dot{\varphi} + \dot{w}(x,t)) + (y_1 + x\theta + v(x,t))(\Omega + \theta\dot{\varphi})\Big]^2\Big\}\Big|_{x=L/2} \\ & + \frac{1}{2}\rho_d h\Big\{J_{pd}\Big[\Omega + \theta\dot{\varphi} + v'(x,t)(-\Omega\theta + \dot{\varphi}) + w'(x,t)(\Omega\varphi + \dot{\theta} + \dot{v}'(x,t))\Big]^2 \\ & - \Omega\theta + \dot{\varphi} - \dot{w}'(x,t)\Big]^2 + I_d\Big[-w'(x,t)(\Omega + \theta\dot{\varphi}) + \Omega\varphi + \dot{\theta} + \dot{v}'(x,t)\Big]^2\Big\}\Big|_{x=L/2}\end{aligned} \tag{13}$$

where ρ_d is disk mass density and m_d, h, I_d and J_{pd} are mass, disk thickness, diametral area moment of inertia and polar area moment of inertia of the disk, respectively. Since the shaft has

© VIBROENGINEERING. JOURNAL OF VIBROENGINEERING. JUNE 2012. VOLUME 14, ISSUE 2. ISSN 1392-8716

a circular cross-section, its polar area moment of inertia is twice its diametrical area moment of inertia. The total kinetic energy of the system is the sum of T_s and T_d.

The strain energy expression due to the bending of the shaft is:

$$\mathrm{U_s} = \frac{1}{2}\int_0^L \left\{ EI\left[(v''(x,t))^2 + (w''(x,t))^2 \right] \right\} dx \tag{14}$$

The strain energy expression of the bearing system is:

$$\begin{aligned} U_b = \frac{1}{2}\sum_i \sum_j k_{ij} q_i q_j = \frac{1}{2}\Big(& k_{y_1y_1} y_1^2 + k_{y_1z_1} y_1 z_1 + k_{z_1y_1} z_1 y_1 + k_{z_1z_1} z_1^2 \\ & + k_{y_2y_2} y_2^2 + k_{y_2z_2} y_2 z_2 + k_{z_2y_2} z_2 y_2 + k_{z_2z_2} z_2^2 \Big) \end{aligned} \tag{15}$$

In addition, the dissipation energy of the shaft system is:

$$D_s = \frac{1}{2}\int_0^L C\left[(\dot{v}(x,t))^2 + (\dot{w}(x,t))^2 \right] dx \tag{16}$$

where C is the external damping coefficient. The dissipation energy of the bearing system is:

$$\begin{aligned} D_b = \frac{1}{2}\sum_i \sum_j C_{ij} \dot{q}_i \dot{q}_j = \frac{1}{2}\Big(& C_{y_1y_1} \dot{y}_1^2 + C_{y_1z_1} \dot{y}_1 \dot{z}_1 + C_{z_1y_1} \dot{z}_1 \dot{y}_1 + C_{z_1z_1} \dot{z}_1^2 \\ & + C_{y_2y_2} \dot{y}_2^2 + C_{y_2z_2} \dot{y}_2 \dot{z}_2 + C_{z_2y_2} \dot{z}_2 \dot{y}_2 + C_{z_2z_2} \dot{z}_2^2 \Big) \end{aligned} \tag{17}$$

To derive the equations of motion, it is convenient to use the assumed mode method for defining displacements as follows:

$$v(x,t) = \sum_{i=1}^{n} \Psi_i(x)\, \mathrm{V}_i(t) = \mathbf{\Psi}^{\mathrm{T}}(x)\, \mathbf{V}(t) \tag{18.a}$$

$$w(x,t) = \sum_{i=1}^{n} \Psi_i(x)\, \mathrm{W}_i(t) = \mathbf{\Psi}^{\mathrm{T}}(x)\, \mathbf{W}(t) \tag{18.b}$$

where n denotes the number of terms in the truncated series expansion, $\mathbf{\Psi}(x)$ is the admissible spatial function vector which describes the transverse deflections of the shaft, and $\mathbf{V}(t)$, $\mathbf{W}(t)$ are the column vectors consisting of the corresponding time-dependent generalized coordinates.

Substituting equation (18) into equations (12-14) and (16), the discrete forms of equations are derived. The Lagrange equations are expressed as:

$$\frac{d}{dt}\left(\frac{\partial T}{\partial \dot{q}_i}\right) - \frac{\partial T}{\partial q_i} + \frac{\partial U}{\partial q_i} + \frac{\partial D}{\partial \dot{q}_i} = Q_i \tag{19}$$

By applying the Lagrange equations and after some mathematical calculations and neglecting small nonlinear terms, the simplified equations of motion can be introduced in compact form as:

$$\mathbf{M}\ddot{\mathbf{q}} + \mathbf{h}(\mathbf{q},\dot{\mathbf{q}}) = \mathbf{Q} \tag{20}$$

where $\mathbf{M}$ is mass matrix, $\mathbf{q} = [\ \mathbf{V}\ \ \mathbf{W}\ \ y_1\ \ \theta\ \ z_1\ \ \varphi\ ]^{\mathbf{T}}$ designates the generalized coordinates vector, and $\mathbf{Q}$ designates the forces vector, that comprises the exciting forces, gravitation and rub-impact forces.

It is assumed that the contact between the rotor (disk) and the stator can be regarded as an elastic impact and the heating effect due to friction is negligible. As shown in Fig. 2, f_n is the radial impact force, f_t is the tangential rub force and φ is the inclination angle between the direction of the impact point and the $Y-$ axis:

$$\begin{cases} f_n = k_s(e-\delta) \\ f_t = \mu f_n \end{cases} \quad e > \delta\ . \tag{21}$$

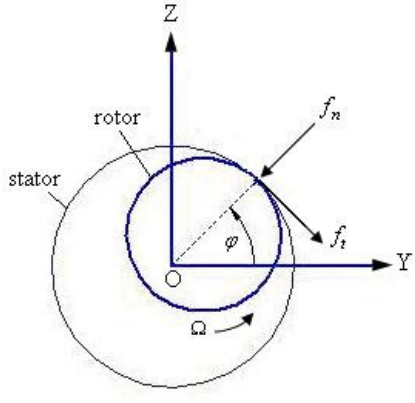

Fig. 2. Schematic diagram of the rub-impact between the rotor and stator

The components of the rub-impact forces in Y and Z directions, i.e. F_Y and F_Z, are:

$$\begin{cases} F_Y = -f_n \cos\varphi + f_t \sin\varphi = -f_n \dfrac{v(x,t)}{e} + f_t \dfrac{w(x,t)}{e} \\ F_Z = -f_n \sin\varphi - f_t \cos\varphi = -f_n \dfrac{w(x,t)}{e} - f_t \dfrac{v(x,t)}{e} \end{cases} \tag{22}$$

where $e = \sqrt{(v(x,t))^2 + (w(x,t))^2}$, μ is the friction coefficient, δ is the radial clearance between the rotor and the stator.

To demonstrate the general method of nonlinear analysis, the case of similar bearings is considered:

$$k_{y_1y_1} = k_{y_2y_2} = k_{yy}/2\ , \quad k_{z_1z_1} = k_{z_2z_2} = k_{zz}/2\ , \quad k_{y_1z_1} = k_{z_1y_1} = k_{yz}/2\ , \quad k_{y_2z_2} = k_{z_2y_2} = k_{zy}/2\ ,$$
$$C_{y_1y_1} = C_{y_2y_2} = C_{yy}/2\ , \ C_{z_1z_1} = C_{z_2z_2} = C_{zz}/2\ , \ C_{y_1z_1} = C_{z_1y_1} = C_{yz}/2\ , \ C_{y_2z_2} = C_{z_2y_2} = C_{zy}/2\ ,$$

where the k_{yy}, k_{yz}, C_{yy}, C_{yz} are the principal and cross-coupling stiffness and damping coefficients, respectively.

Let us define the non-dimensional parameters and constant coefficients as:

© VIBROENGINEERING. JOURNAL OF VIBROENGINEERING. JUNE 2012. VOLUME 14, ISSUE 2. ISSN 1392-8716

$$\hat{\mathbf{v}}=\frac{\mathbf{V}}{\delta},\quad \hat{\mathbf{w}}=\frac{\mathbf{W}}{\delta},\quad \hat{y}_1=\frac{y_1}{\delta},\quad \hat{z}_1=\frac{z_1}{\delta},\quad \tau=\Omega t,\quad \frac{d}{dt}=\Omega\frac{d}{d\tau},\quad S=\frac{\Omega}{\omega_n},\quad \alpha_1=\frac{m_d}{\rho A},\quad \alpha_2=\frac{m_d L}{\rho A\delta},$$

$$\alpha_3=\frac{m_d L\delta}{\rho A},\quad \alpha_4=\frac{m_d L^2}{\rho A},\quad \alpha_5=\frac{m_d\delta^2}{\rho A},\quad \beta_1=\frac{I_s}{A},\quad \beta_2=\frac{I_s}{A\delta},\quad \gamma_1=\frac{\rho_d\, h\, I_d}{\rho A},\quad \gamma_2=\frac{\rho_d\, h\, I_d}{\rho A\delta},$$

$$\zeta=\frac{C}{2\sqrt{\rho A(EI_s/l^4)}},\qquad \xi_{yy}=\frac{C_{yy}}{2\sqrt{\rho ALk_{yy}}},\qquad \xi_{zz}=\frac{C_{zz}}{2\sqrt{\rho ALk_{zz}}},\qquad \xi_{yz}=\frac{C_{yz}}{2\sqrt{\rho ALk_{yz}}},$$

$$\xi_{zy}=\frac{C_{zy}}{2\sqrt{\rho ALk_{zy}}},\quad \omega_{yy}=\sqrt{\frac{k_{yy}}{2\rho AL}},\quad \omega_{zz}=\sqrt{\frac{k_{zz}}{2\rho AL}},\quad \omega_{yz}=\sqrt{\frac{k_{yz}}{2\rho AL}},\quad \omega_{zy}=\sqrt{\frac{k_{zy}}{2\rho AL}},$$

$$\omega_n^2=\frac{EI_s}{\rho Al^4},\ S_{yy}=\frac{\omega_{yy}}{\Omega},\ S_{zz}=\frac{\omega_{zz}}{\Omega},\ S_{yz}=\frac{\omega_{yz}}{\Omega},\ S_{zy}=\frac{\omega_{zy}}{\Omega},\ p=\rho A\delta\Omega^2.$$

Now, one can rewrite the simplified non-dimensional form of equation (20) as:

$$\hat{\mathbf{M}}\ddot{\hat{\mathbf{q}}}+\hat{\mathbf{h}}(\hat{\mathbf{q}},\dot{\hat{\mathbf{q}}})=\hat{\mathbf{Q}} \tag{23}$$

where $\hat{\mathbf{M}}$ and $\hat{\mathbf{h}}$ presented in Appendix A.

Equation (23) describes the coupled nonlinear differential equation governing the flexible shaft-disk motion.

Introducing $\mathbf{q}=\mathbf{z}_1$ and $\dot{\mathbf{q}}=\mathbf{z}_2$, the equation (23) can then be rewritten as the following set of first-order differential equations:

$$\begin{cases}\dot{\mathbf{z}}_1=\mathbf{z}_2\\ \dot{\mathbf{z}}_2=\hat{\mathbf{M}}^{-1}(\hat{\mathbf{Q}}-\hat{\mathbf{h}}(\mathbf{z}_1,\mathbf{z}_2))\end{cases} \tag{24}$$

3. Numerical Results and Discussion

The numerical analysis of equation (24) is carried out by a variable step solver based on the Runge-Kutta formulation. The main point in obtaining reliable results is to select proper time steps for the numerical integration as well as proper number of modes for the continuous system [22]. In this work, a variable time step and three modes are used for numerical analysis. Numerical results demonstrated that the use of three modes guarantees the convergence of numerical results. The non-dimensional speed ratio S is used as a control parameter. The mode shapes of the non-rotating uniform beam with simply supported boundary conditions at both ends are used as the admissible functions for the flexible shaft-disk system [23], i.e.:

$$\Psi_i(x)=\sqrt{2}\sin(\frac{i\pi x}{L}),\ i=1,2,3,\ldots \tag{25}$$

To guarantee that the data being used are in a steady state, the first few hundred-time series data of the integration have been neglected. The results of the next few hundred time series are retained to carry out the analysis.

The values for the constant and non-dimensional parameters of the system used in the analysis are:

$\alpha_1 = 0.35(m)$, $\alpha_2 = 882.9(m)$, $\alpha_3 = 1.4\times10^{-4}(m^3)$, $\alpha_4 = 0.35(m^3)$, $\alpha_5 = 5.6\times10^{-8}(m^3)$, $\beta_1 = 5.6\times10^{-5}(m^2)$, $\beta_2 = 0.14(m)$, $\gamma_1 = 2.01\times10^{-3}(m^3)$, $\gamma_2 = 5.02(m^2)$, $\zeta = 0.372$.

The numerical simulation is carried out for the following cases (subsections 3.1 – 3.6).

3.1. Simply supported end conditions

In this case, the end-supports of the shaft-disk system are considered as simply supported. The speed ratio S was selected as the control parameter. Five different techniques namely, time series, phase plane portrait, power spectrum, Poincaré map, bifurcation diagrams, and Lyapunov exponents are applied to analyze the dynamic behavior of the system.

To generate the bifurcation diagram, the system control parameter (i.e. speed ratio (S)) is varied with a fixed step and the state variables at the end of each step are used as initial conditions for the next step. These data points are then plotted versus the rotational speed ratio. If the motion is regular (periodic) at the specific rotational speed ratio, the bifurcation diagram should contain finite number of separate points. When the motion is quasi-periodic or chaotic, the data points in the bifurcation diagram are distributed along a line.

The bifurcation diagram of the system with simply supported end-condition is shown in Fig. 3.1. In this case, the dynamic behavior of the system is regular with period-one ($1T$) until $S = 6.026$. The period doubling is observed at $S = 6.028$. This situation is maintained up to $S = 6.09$. Again, the motion returns to period $1T$ at $S = 6.092$.

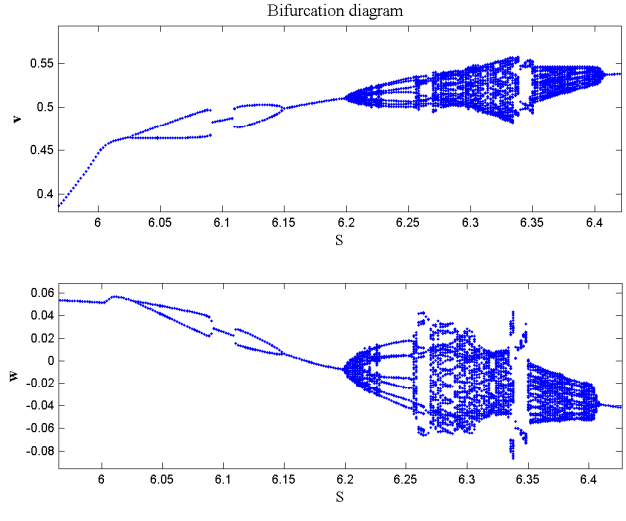

Fig. 3.1. Bifurcation diagram of the system with simply supported end-conditions

The behavior of the system at $S = 6.108$, jumps to a different regular attractor with period-two. Since the system response jumps to a remote attractor, the bifurcation point can be classified as a dangerous bifurcation [24]. In the region $S = [6.15\sim6.198]$, the motion has period one. The motion of the system becomes irregular (quasi-periodic or chaotic) at $S = [6.2\sim6.228]$. The motion of the system becomes sub-harmonic with period ($7T$) at $S = [6.23\sim6.254]$. The second irregular region appears at $S = [6.256\sim6.258]$. The regular sub-harmonics with period ($11T$) and ($4T$) are captured at $S = [6.26\sim6.268]$. The bifurcation diagram shows two rather large irregular regions at intervals $S = [6.27\sim6.338]$ and $S = [6.342\sim6.408]$. The regular motions with

period ($2T$) and ($4T$) are captured at $S=[6.26\sim6.268]$. The behavior of the system alternates between regular ($1T$) and irregular motions at $S=[6.35\sim6.452]$. It gets into the sub-harmonic motion with period-one ($1T$) at $S=[6.454\sim6.784]$ with some small oscillations. Finally, it returns back into irregular motion at $S=6.786$.

Fig. 3.2 provides time series, phase plane portrait, power spectrum and Poincaré map at $S=6.34$. The dynamic response of the system demonstrates the sub-harmonic motion of period $4T$. As shown in Fig. 3.2(c), the power spectrum at this speed ratio has a clear peak at the frequencies 1/4 and the four discrete points in the Poincaré map shown in Fig. 3.2(d) confirm the sub-harmonic (period-4) motion.

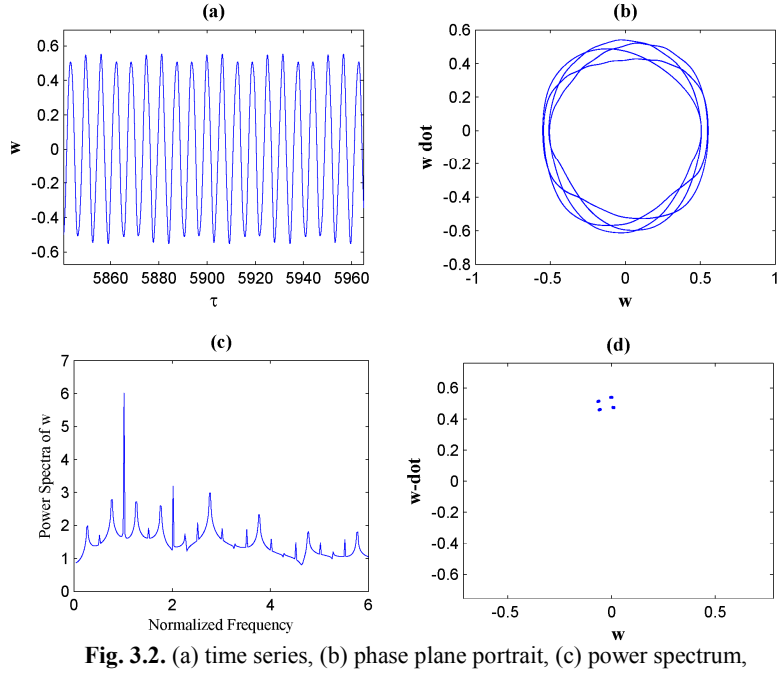

Fig. 3.2. (a) time series, (b) phase plane portrait, (c) power spectrum, (d) Poincaré map with simply supported end-conditions at $S=6.34$

3.2. Similar bearings with constant coefficients

The bifurcation diagram of the system with similar bearings at its two ends is shown in Fig. 4.1. In this case, the dynamic behavior of the system is regular with period-one ($1T$) until $S=5.728$. The rub-impact occurs at $S=5.729$ with period doubling bifurcation. This situation is maintained up to $S=5.761$. Again, the motion returns to period $1T$ at $S=[5.762\sim5.819]$. The motion of the system becomes irregular (quasi-periodic or chaotic) at $S=[5.82\sim5.85]$, that accompanied with increases in the response amplitude. The response amplitude decreases at $S=5.851$ and the second irregular region appears at $S=[5.851\sim5.903]$. The regular sub-harmonics with period ($4T$) and ($3T$) are captured at $S=[5.904\sim5.906]$. The motion becomes irregular at $S=[5.907\sim5.911]$. The regular motions with period ($5T$) and ($4T$) are captured at $S=[5.912\sim5.947]$. The bifurcation diagram shows the other rather large irregular regions at interval $S=[5.948\sim5.982]$. The behavior gets into the sub-harmonic motion with period one ($1T$) at $S=5.983$.

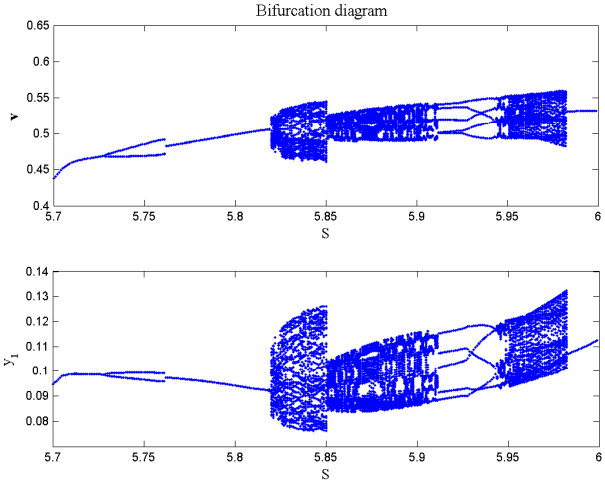

Fig. 4.1. Bifurcation diagram of the system with similar bearing coefficients

Fig. 4.2 shows the time series, phase plane portrait, power spectrum and Poincaré map at $S = 5.75$. The behavior of the system demonstrates the sub-harmonic motion of period $2T$. As illustrated in Fig. 4.2(c), the power spectrum at this speed ratio has a clear peak at the frequencies 1/2 and the two discrete points in the Poincaré map shown in Fig. 4.2(d) confirm the sub-harmonic (period-2) motion. Fig. 4.3 shows the dynamic response of the system at $S = 5.84$. As shown in Figs. 4.3(b, d), many crossings and loops are seen in the phase plane portrait and fractal structure in Poincaré map, which can be a sign of the chaotic motion.

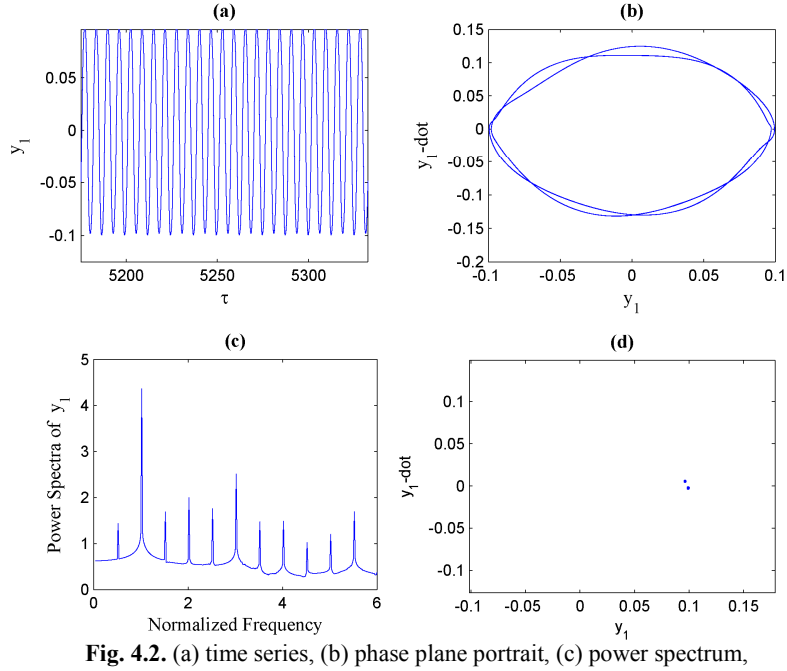

Fig. 4.2. (a) time series, (b) phase plane portrait, (c) power spectrum, (d) Poincaré map with similar bearing coefficients at $S = 5.75$

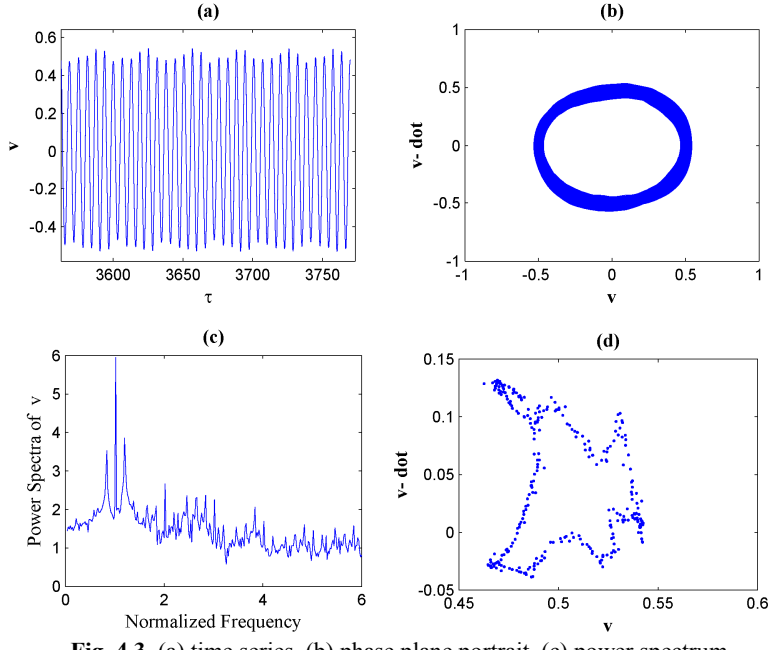

Fig. 4.3. (a) time series, (b) phase plane portrait, (c) power spectrum, (d) Poincaré map with similar bearing coefficients at $S = 5.84$

3.3. Principal stiffness coefficient effect

In this case study, the speed ratio is constant, i.e. $S = 5.85$, as mentioned above, the dynamic behavior of the system is chaotic. The aim of this case is to investigate the effect of principal stiffness on the chaotic behavior of the system. Fig. 5.1 shows the bifurcation diagram of the system when S_{yy} is selected as a control parameter. The behavior of the system is irregular up to $S_{yy} = 9.058$. By increasing the control parameter, the response gets to regular motion with period ($5T$) at $S_{yy} = [9.059\sim9.062]$ and return to irregular one at $S_{yy} = [9.063\sim9.221]$. Again, the motion returns to period $5T$ at $S_{yy} = 9.222$ and this region continues up to $S_{yy} = 9.306$. By further increasing the stiffness of the bearings, the other irregular region appears at $S_{yy} = [9.307\sim9.341]$. The motion returns to period $1T$ at $S_{yy} = 9.342$, thus properly choosing the principal stiffness coefficient and its respective parameter can improve the dynamic behavior of the system and avoid the chaotic behavior at $S = 5.85$.

Fig. 5.2 shows the time series, phase plane portrait, power spectrum and Poincaré map at $S_{yy} = 9.24$. The behavior of the system demonstrates the sub-harmonic motion of period $5T$. As shown in Fig. 5.2(c), the power spectrum at this speed ratio has a clear peak at the frequencies 1/5 and the five discrete points in the Poincaré map shown in Fig. 2.2(d) confirm the sub-harmonic (period-5) motion at bearing position. Fig. 5.3 shows the dynamic response of the system at $S_{yy} = 9.45$. As shown in Fig. 5.3(d), there is single point in the Poincaré map; this can be a sign of the regular motion with period one ($1T$).

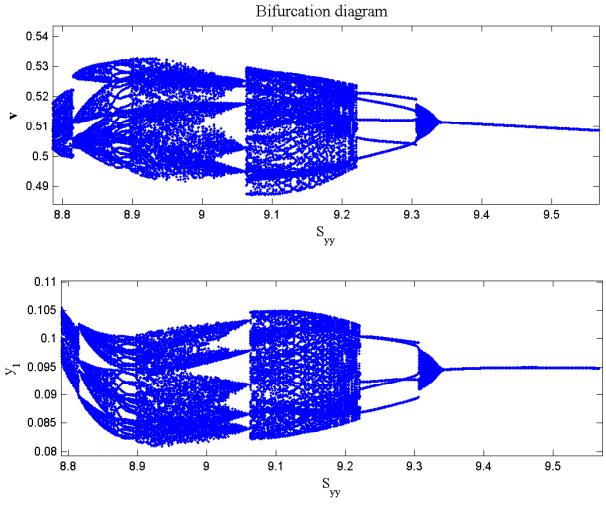

Fig. 5.1. Bifurcation diagram of the system for principle stiffness coefficient

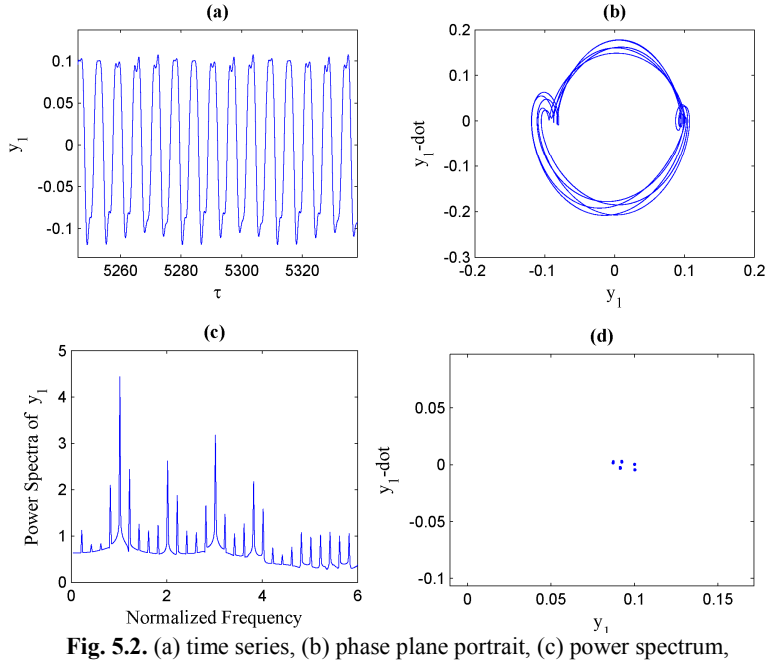

Fig. 5.2. (a) time series, (b) phase plane portrait, (c) power spectrum, (d) Poincaré map with principle stiffness coefficient at $S_{yy} = 9.24$

3.4. Cross-coupling stiffness coefficient effect

For this case study, the speed ratio is constant, i.e. $S = 4.5$, as mentioned in section 3.2, the dynamic behavior of the system is regular ($1T$) until $S = 5.728$. The aim of this case is to investigate the effect of cross-coupling stiffness on the behavior of the system. The Fig. 6.1 shows the bifurcation diagram of the system with cross-coupling stiffness coefficient while S_{zy} is selected as a control parameter. The behavior of the system is regular with period one up to

$S_{zy} = 7.96$. Increasing the cross-coupling stiffness will increase the disorder behavior of the system. The motion gets into chaotic behavior at $S_{zy} = 7.97$. The situation preserves until $S_{zy} = 8.06$ accompanying with amplitude increasing. By further increasing the control parameter, the irregular motion aggravates. Thus increasing the cross-coupling stiffness can lead to undesirable behavior, even if the speed ratio is in the regular motion region.

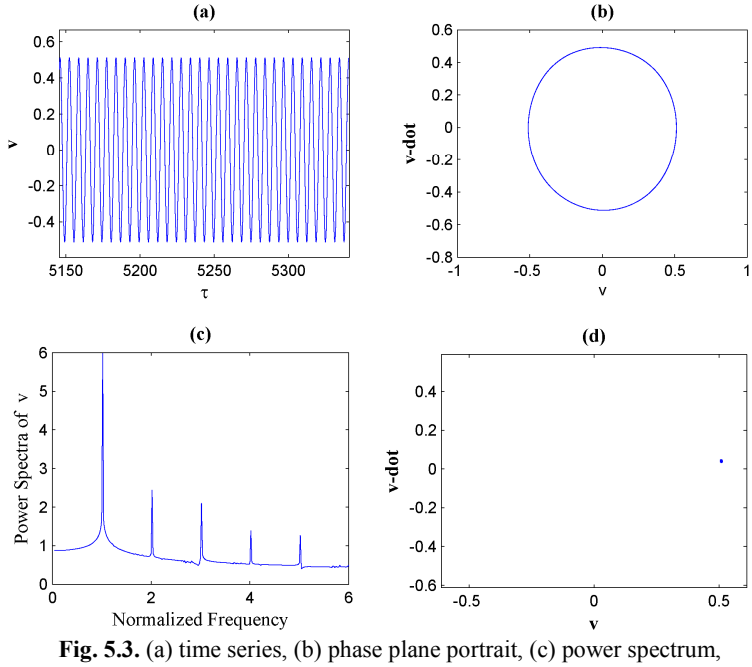

Fig. 5.3. (a) time series, (b) phase plane portrait, (c) power spectrum, (d) Poincaré map with principle stiffness coefficient at $S_{yy} = 9.45$

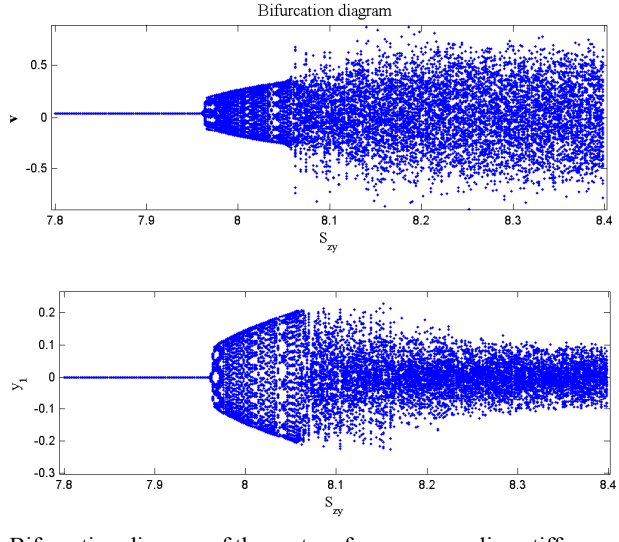

Fig. 6.1. Bifurcation diagram of the system for cross coupling stiffness coefficient

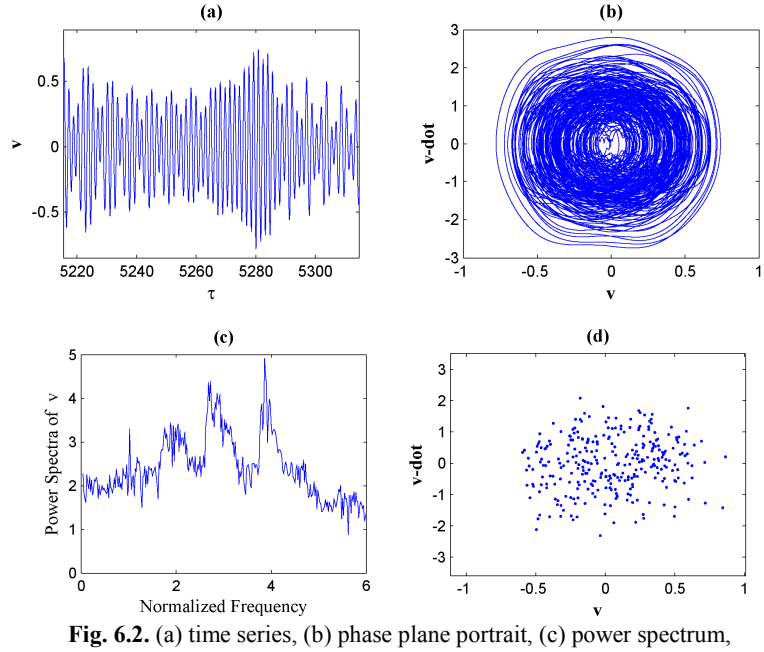

Fig. 6.2. (a) time series, (b) phase plane portrait, (c) power spectrum, (d) Poincaré map with cross coupling stiffness coefficient at $S_{zy} = 8.2$

Fig. 6.2 shows the dynamic response of the system at $S_{zy} = 8.2$. As indicated, many crossings and loops in the phase plane portrait, broadband power spectrum and fractal structure in Poincaré map are observed, which can be a sign of the chaotic motion.

3.5. Principal damping coefficient effect

In this case study, the speed ratio is constant, i.e. $S = 5.85$, in which the system behavior is in a chaotic region. The effect of principal damping on the dynamic behavior of the system is studied in this section. Fig. 7.1 displays the bifurcation diagram of the system while the principal damping coefficient ξ_{yy} is selected as a control parameter. The behavior of the system is regular ($3T$) until $\xi_{yy} = 0.017$. By increasing the control parameter, the response falls into chaotic motion at $\xi_{yy} = [0.018 \sim 0.052]$ and returns to regular motion with period ($5T$) again at $\xi_{yy} = [0.115 \sim 0.140]$. By further increasing the principal-damping ratio, the motion returns to period $1T$ at $\xi_{yy} = 0.150$. Thus by proper selection of the principal damping ratio one can improve the dynamic behavior of the system and avoid the chaotic behavior at $S = 5.85$.

Fig. 7.2 shows the time series, phase plane portrait, power spectrum and Poincaré map at $\xi_{yy} = 0.012$. As shown, many crossings and loops in the phase plane portrait, broadband power spectrum and fractal structure in Poincaré map are observed, which can be a sign of the chaotic motion in the bearing position. As shown in Fig. 7.3, at $\xi_{yy} = 0.06$, the behavior of the system demonstrates the sub-harmonic motion of period $5T$.

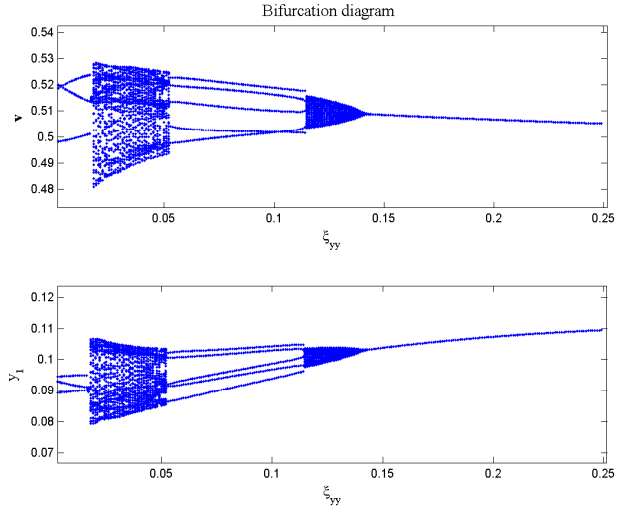

Fig. 7.1. Bifurcation diagram of the system for principle damping coefficient

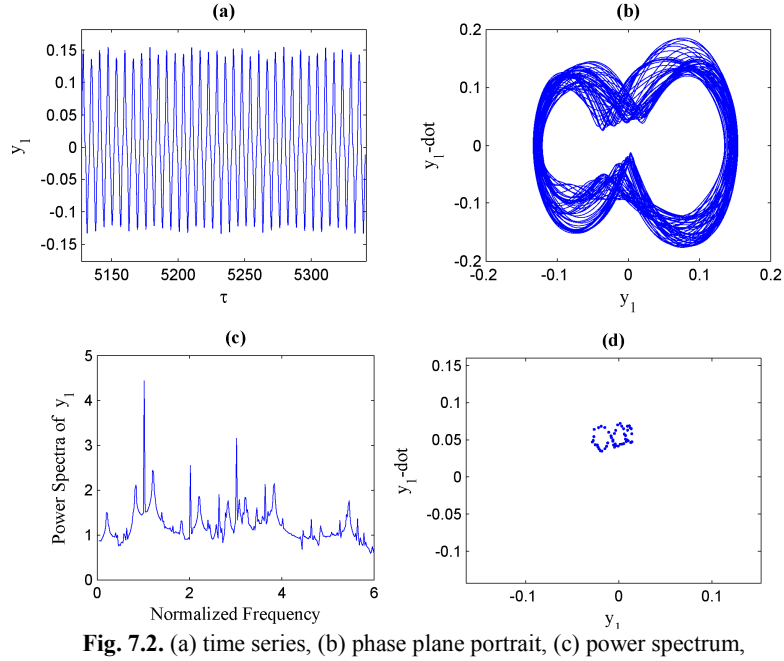

Fig. 7.2. (a) time series, (b) phase plane portrait, (c) power spectrum, (d) Poincaré map with principle damping coefficient at $\xi_{yy} = 0.012$

3.6. Cross-coupling damping coefficient effect

In this case, the speed ratio is constant, i.e. $S = 4.5$, as mentioned previously, the motion is regular ($1T$) until $S = 5.728$. Fig. 8.1 shows the bifurcation diagram of the system with cross coupling damping coefficient ξ_{zy} as the control parameter. The behavior of the system is regular with period until $\xi_{zy} = 0.198$. Increasing the cross-coupling damping coefficient will increase the disorder behavior of the system. The motion gets into chaotic behavior at $S_{zy} = 0.199$. By

further increasing the control parameter, the irregular motion aggravates. Thus increasing the cross-coupling damping coefficient can lead to undesirable behavior, even if the speed ratio is in the regular motion region.

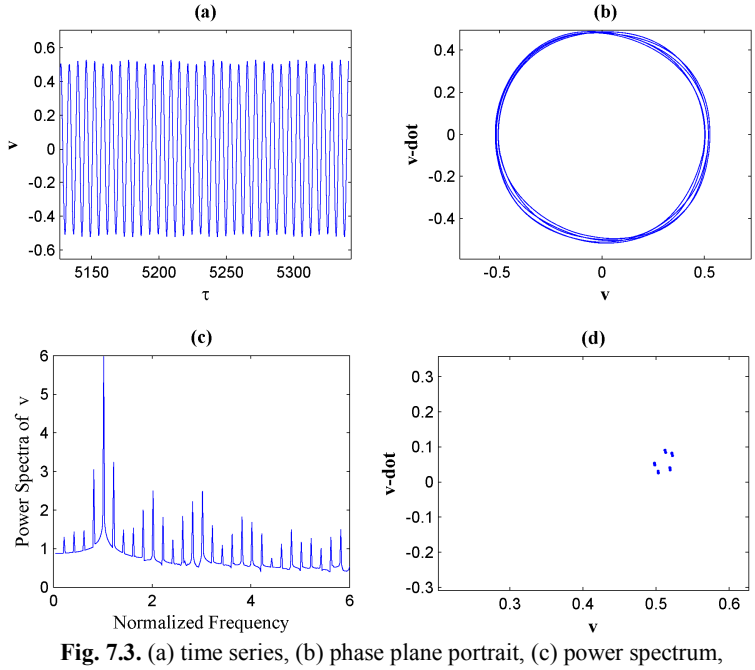

Fig. 7.3. (a) time series, (b) phase plane portrait, (c) power spectrum, (d) Poincaré map with principle damping coefficient at $\xi_{yy} = 0.06$

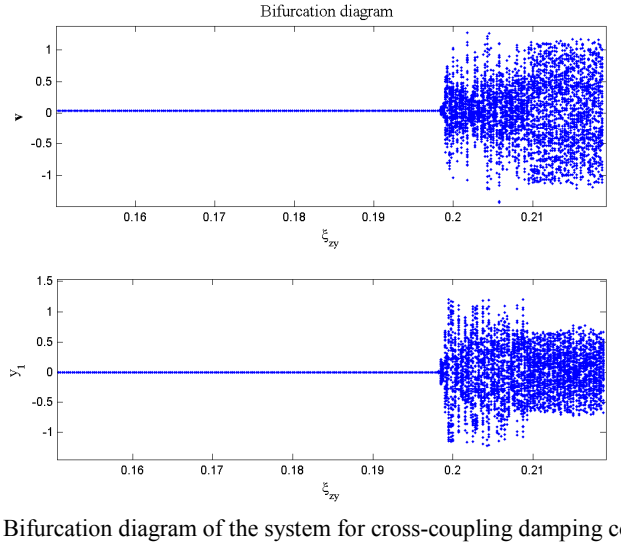

Fig. 8.1. Bifurcation diagram of the system for cross-coupling damping coefficient

Fig. 8.2 shows the dynamic response of the system at $\xi_{zy} = 0.21$. As shown, many crossings and loops in the phase plane portrait, broadband power spectrum and geometrically fractal structure in Poincaré map are observed, which can be a sign of the chaotic motion.

© VIBROENGINEERING. JOURNAL OF VIBROENGINEERING. JUNE 2012. VOLUME 14, ISSUE 2. ISSN 1392-8716

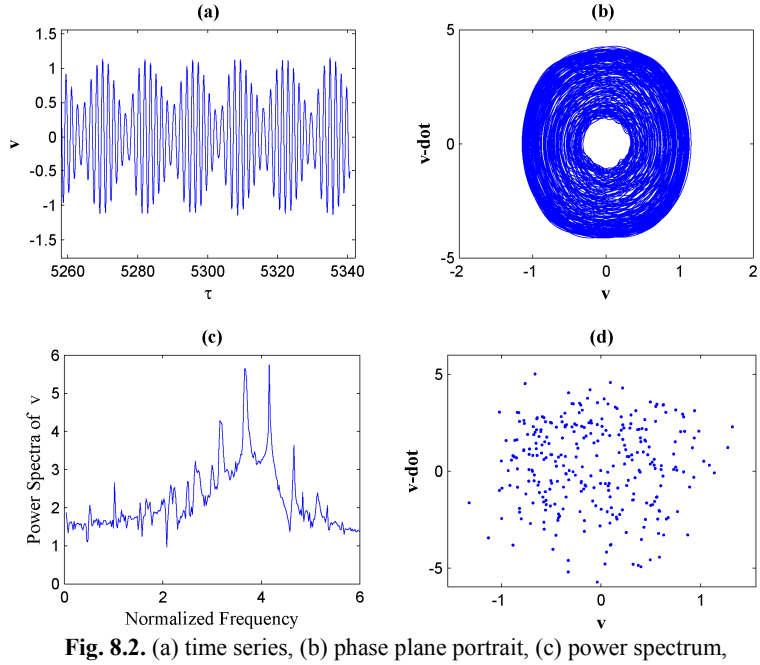

Fig. 8.2. (a) time series, (b) phase plane portrait, (c) power spectrum, (d) Poincaré map with cross-coupling damping coefficient at $\xi_{zy} = 0.21$

The Lyapunov exponents determine the average rate of the exponential expansion or contraction in the direction of an initial deviation $y(0)$ on a trajectory of the system, which is given by $\bar{\lambda}_i = \lim_{t\to\infty} \frac{1}{t} \ln(\frac{\|y(t)\|}{\|y(0)\|})$, where the symbol $\| \ \|$ denotes a vector norm and $\bar{\lambda}_i$ is called the Lyapunov exponent. If the maximum Lyapunov exponent is negative or zero, there is a regular motion, and a positive maximum Lyapunov exponent will confirm the chaotic motion [24, 25]. The Lyapunov exponents of Eq. (23) are obtained using the algorithm given in Ref. [26]. As shown in Fig. 9, the maximum Lyapunov exponents at $S = 5.84$, $S_{zy} = 8.2$, $\xi_{yy} = 0.012$ and $\xi_{zy} = 0.21$ in the respective cases are positive, confirming the chaotic motion at given control parameters. Thus, the maximum Lyapunov exponent proves as a useful tool for verifying the results of other nonlinear analytical tools used to identify chaotic behavior.

4. Conclusion

The influence of end-supports conditions on the chaos and bifurcation of a rotating flexible shaft-disk system with rub-impact was investigated in this paper. The system was modeled as a continuous shaft with a rigid disk in its mid span and the end-supports modeled as eight-coefficient bearings. The assumed mode method was used to discretize the partial differential equations of motion. Time series, phase plane portrait, Poincaré map, bifurcation diagrams, and Lyapunov exponents were used to analyze the nonlinear dynamic behavior of the system. The effects of Coriolis and centrifugal forces due to shaft flexibility were also considered. The results obtained from the different numerical tools agreed well with each other. According to the results, the following conclusions may be drawn:

© VIBROENGINEERING. JOURNAL OF VIBROENGINEERING. JUNE 2012. VOLUME 14, ISSUE 2. ISSN 1392-8716

1. Considering the end-supports as eight-coefficients bearing can primarily change the speed ratios in which rub-impact occurs, i.e. simply supported $S = 6.028$ and eight-coefficient similar bearing $S = 5.728$. In addition, the dynamic behavior of the system had substantial differences in the two mentioned cases.

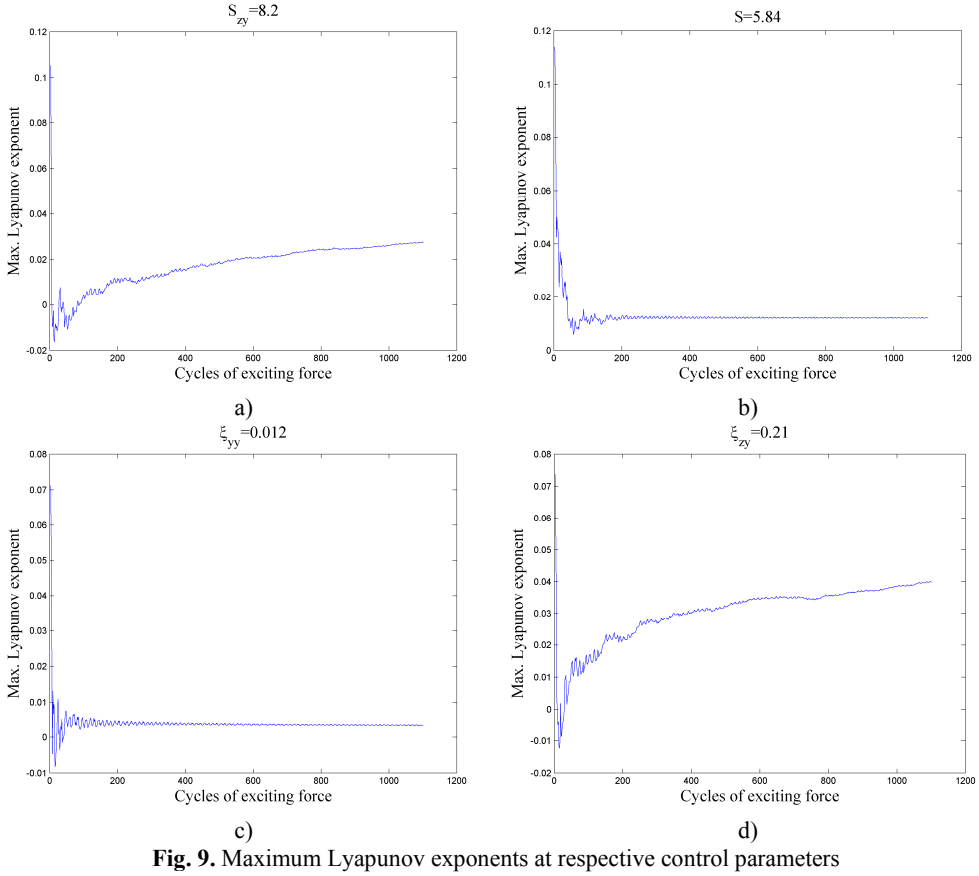

Fig. 9. Maximum Lyapunov exponents at respective control parameters

2. The principal stiffness and damping coefficients can improve the dynamic behavior of the system. As demonstrated, by increasing these coefficients, the chaotic vibration at $S = 5.85$ transformed into the period-one motion.

3. The cross-coupling stiffness and damping coefficients can aggravate the dynamic behavior of the system. As demonstrated, by increasing these coefficients, the regular motion with period one at $S = 4.50$ transformed to the chaotic vibrations.

Thus, the results obtained in this study allow a suitable set of system parameters (i.e., principal and cross-coupling stiffness and damping coefficients) to be specified such that the rotating system trajectories avoid undesirable behavior and thereby lead to increase of the life cycle of the system.

© VIBROENGINEERING. JOURNAL OF VIBROENGINEERING. JUNE 2012. VOLUME 14, ISSUE 2. ISSN 1392-8716

Appendix A

$$\hat{\mathbf{M}}=\begin{bmatrix}\left[\hat{\mathbf{M}}_{v1}\right]_{n\times n} & \left[\hat{\mathbf{M}}_{v2}\right]_{n\times n} & \left[\hat{\mathbf{M}}_{v3}\right]_{n\times 1} & \left[\hat{\mathbf{M}}_{v4}\right]_{n\times 1} & \left[\hat{\mathbf{M}}_{v5}\right]_{n\times 1} & \left[\hat{\mathbf{M}}_{v6}\right]_{n\times 1}\\ \left[\hat{\mathbf{M}}_{w1}\right]_{n\times n} & \left[\hat{\mathbf{M}}_{w2}\right]_{n\times n} & \left[\hat{\mathbf{M}}_{w3}\right]_{n\times 1} & \left[\hat{\mathbf{M}}_{w4}\right]_{n\times 1} & \left[\hat{\mathbf{M}}_{w5}\right]_{n\times 1} & \left[\hat{\mathbf{M}}_{w6}\right]_{n\times 1}\\ \left[\hat{\mathbf{M}}_{y1}\right]_{1\times n} & \left[\hat{\mathbf{M}}_{y2}\right]_{1\times n} & \left[\hat{\mathbf{M}}_{y3}\right]_{1\times 1} & \left[\hat{\mathbf{M}}_{y4}\right]_{1\times 1} & \left[\hat{\mathbf{M}}_{y5}\right]_{1\times 1} & \left[\hat{\mathbf{M}}_{y6}\right]_{1\times 1}\\ \left[\hat{\mathbf{M}}_{\theta 1}\right]_{1\times n} & \left[\hat{\mathbf{M}}_{\theta 2}\right]_{1\times n} & \left[\hat{\mathbf{M}}_{\theta 3}\right]_{1\times 1} & \left[\hat{\mathbf{M}}_{\theta 4}\right]_{1\times 1} & \left[\hat{\mathbf{M}}_{\theta 5}\right]_{1\times 1} & \left[\hat{\mathbf{M}}_{\theta 6}\right]_{1\times 1}\\ \left[\hat{\mathbf{M}}_{z1}\right]_{1\times n} & \left[\hat{\mathbf{M}}_{z2}\right]_{1\times n} & \left[\hat{\mathbf{M}}_{z3}\right]_{1\times 1} & \left[\hat{\mathbf{M}}_{z4}\right]_{1\times 1} & \left[\hat{\mathbf{M}}_{z5}\right]_{1\times 1} & \left[\hat{\mathbf{M}}_{z6}\right]_{1\times 1}\\ \left[\hat{\mathbf{M}}_{\varphi 1}\right]_{1\times n} & \left[\hat{\mathbf{M}}_{\varphi 2}\right]_{1\times n} & \left[\hat{\mathbf{M}}_{\varphi 3}\right]_{1\times 1} & \left[\hat{\mathbf{M}}_{\varphi 4}\right]_{1\times 1} & \left[\hat{\mathbf{M}}_{\varphi 5}\right]_{1\times 1} & \left[\hat{\mathbf{M}}_{\varphi 6}\right]_{1\times 1}\end{bmatrix} \tag{A.1}$$

where the mass matrix elements are as:

$$\hat{\mathbf{M}}_{\mathrm{v1}}=\hat{\mathbf{M}}_{\mathrm{w2}}=\mathbf{I}+\alpha_1\boldsymbol{\Gamma}_1^{-1}\boldsymbol{\Gamma}_{\mathrm{d1}},\ \hat{\mathbf{M}}_{\mathrm{v2}}=\hat{\mathbf{M}}_{\mathrm{w1}}=\mathbf{0},\ \hat{\mathbf{M}}_{\mathrm{v3}}=\hat{\mathbf{M}}_{\mathrm{w5}}=\boldsymbol{\Gamma}_1^{-1}\boldsymbol{\Gamma}_5+\alpha_1\boldsymbol{\Gamma}_1^{-1}\boldsymbol{\Gamma}_{\mathrm{d3}},$$

$$\hat{\mathbf{M}}_{\mathrm{v4}}=\hat{\mathbf{M}}_{\mathrm{w6}}=\frac{1}{\delta}\boldsymbol{\Gamma}_1^{-1}\boldsymbol{\Gamma}_4+\frac{\alpha_2}{2}\boldsymbol{\Gamma}_1^{-1}\boldsymbol{\Gamma}_{\mathrm{d3}},\ \hat{\mathbf{M}}_{\mathrm{v5}}=\hat{\mathbf{M}}_{\mathrm{v6}}=\hat{\mathbf{M}}_{\mathrm{w3}}=\hat{\mathbf{M}}_{\mathrm{w4}}=\mathbf{0},$$

$$\hat{\mathbf{M}}_{y1}=\hat{\mathbf{M}}_{z2}=\Gamma_{6-1}^{-1}\boldsymbol{\Gamma}_9+\alpha_1\Gamma_{6-1}^{-1}\boldsymbol{\Gamma}_{\mathrm{d5}},\ \hat{\mathbf{M}}_{y2}=\hat{\mathbf{M}}_{z1}=\hat{\mathbf{M}}_{\theta 2}=\hat{\mathbf{M}}_{\varphi 1}=\mathbf{0},\ \hat{\mathbf{M}}_{y3}=\hat{\mathbf{M}}_{z4}=1+\alpha_1\Gamma_{6-1}^{-1},$$

$$\hat{\mathbf{M}}_{y4}=\hat{\mathbf{M}}_{z6}=\frac{1}{\delta}\Gamma_{6-1}^{-1}\Gamma_{6-2}+\frac{\alpha_2}{2}\Gamma_{6-1}^{-1},$$

$$\hat{\mathbf{M}}_{y5}=\hat{\mathbf{M}}_{y6}=\hat{\mathbf{M}}_{z3}=\hat{\mathbf{M}}_{z4}=\hat{\mathbf{M}}_{\theta 5}=\hat{\mathbf{M}}_{\theta 6}=\hat{\mathbf{M}}_{\varphi 3}=\hat{\mathbf{M}}_{\varphi 4}=0,$$

$$\hat{\mathbf{M}}_{\theta 1}=\hat{\mathbf{M}}_{\varphi 2}=\delta\Gamma_7^{-1}\boldsymbol{\Gamma}_{10}+\frac{\alpha_3}{2}\Gamma_7^{-1}\boldsymbol{\Gamma}_{\mathrm{d5}},\ \hat{\mathbf{M}}_{\theta 3}=\hat{\mathbf{M}}_{\varphi 5}=\delta\Gamma_7^{-1}\Gamma_{6-2}+\frac{\alpha_3}{2}\Gamma_7^{-1},$$

$$\hat{\mathbf{M}}_{\theta 4}=\hat{\mathbf{M}}_{\varphi 6}=1+\frac{\alpha_4}{4}\Gamma_7^{-1},$$

$$\hat{\mathbf{H}}=\hat{\mathbf{Q}}-\hat{\mathbf{h}}=[\,\hat{\mathbf{H}}_v(\hat{\mathbf{q}},\dot{\hat{\mathbf{q}}})\quad\hat{\mathbf{H}}_w(\hat{\mathbf{q}},\dot{\hat{\mathbf{q}}})\quad\hat{\mathbf{H}}_{y1}(\hat{\mathbf{q}},\dot{\hat{\mathbf{q}}})\quad\hat{\mathbf{H}}_\theta(\hat{\mathbf{q}},\dot{\hat{\mathbf{q}}})\quad\hat{\mathbf{H}}_{z1}(\hat{\mathbf{q}},\dot{\hat{\mathbf{q}}})\quad\hat{\mathbf{H}}_\varphi(\hat{\mathbf{q}},\dot{\hat{\mathbf{q}}})\,]^{\mathrm{T}} \tag{A.2}$$

$$\begin{aligned}\hat{\mathbf{H}}_{\mathrm{v}}=&\frac{\boldsymbol{\Gamma}_1^{-1}\mathbf{Q}_v}{\mathrm{p}}-[-\boldsymbol{\Gamma}_1^{-1}\boldsymbol{\Gamma}_5\left(2\dot{\hat{z}}_1+\hat{\theta}\hat{\varphi}\hat{z}_1+\hat{\varphi}^2\hat{y}_1+\hat{y}_1\right)-\frac{1}{\delta}\boldsymbol{\Gamma}_1^{-1}\boldsymbol{\Gamma}_4\left(2\dot{\hat{\varphi}}+2\hat{\varphi}^2\hat{\theta}+\hat{\theta}\right)\\&-2\dot{\hat{\mathbf{w}}}-\hat{\varphi}\hat{\theta}\,\hat{\mathbf{w}}-\hat{\varphi}^2\hat{\mathbf{v}}-\hat{\mathbf{v}}+\frac{2\zeta}{S}\dot{\hat{\mathbf{v}}}+\frac{2L^4}{S^2}\boldsymbol{\Gamma}_1^{-1}\boldsymbol{\Gamma}_3\hat{\mathbf{v}}-\beta_1\boldsymbol{\Gamma}_1^{-1}\boldsymbol{\Gamma}_2\hat{\mathbf{v}}-\beta_2\boldsymbol{\Gamma}_1^{-1}\boldsymbol{\Gamma}_8\hat{\theta}\\&-\alpha_1\boldsymbol{\Gamma}_1^{-1}\boldsymbol{\Gamma}_{\mathrm{d3}}\left(2\dot{\hat{z}}_1+\hat{\theta}\hat{\varphi}\hat{z}_1+\hat{\varphi}^2\hat{y}_1+\hat{y}_1\right)-\alpha_1\boldsymbol{\Gamma}_1^{-1}\boldsymbol{\Gamma}_{\mathrm{d1}}\left(2\dot{\hat{\mathbf{w}}}+\hat{\varphi}\hat{\theta}\,\hat{\mathbf{w}}+\hat{\varphi}^2\hat{\mathbf{v}}+\hat{\mathbf{v}}\right)\\&-\frac{\alpha_2}{2}\boldsymbol{\Gamma}_1^{-1}\boldsymbol{\Gamma}_{\mathrm{d3}}\left(2\dot{\hat{\varphi}}+2\hat{\varphi}^2\hat{\theta}+\hat{\theta}\right)-\gamma_1\boldsymbol{\Gamma}_1^{-1}\boldsymbol{\Gamma}_{\mathrm{d2}}\hat{\mathbf{v}}+\gamma_2\boldsymbol{\Gamma}_1^{-1}\boldsymbol{\Gamma}_{\mathrm{d4}}\hat{\theta}]\end{aligned} \tag{A.3}$$

$$\begin{aligned}\hat{\mathbf{H}}_{\mathrm{w}}=&\frac{\boldsymbol{\Gamma}_1^{-1}\mathbf{Q}_w}{\mathrm{p}}-[\boldsymbol{\Gamma}_1^{-1}\boldsymbol{\Gamma}_5\left(2\dot{\hat{y}}_1-\hat{\theta}\hat{\varphi}\hat{y}_1-\hat{\theta}^2\hat{z}_1-\hat{z}_1\right)+\frac{1}{\delta}\boldsymbol{\Gamma}_1^{-1}\boldsymbol{\Gamma}_4\left(2\dot{\hat{\theta}}-2\hat{\varphi}\hat{\theta}^2-\hat{\varphi}\right)\\&+2\dot{\hat{\mathbf{v}}}-\hat{\varphi}\hat{\theta}\,\hat{\mathbf{v}}-\hat{\theta}^2\hat{\mathbf{w}}-\hat{\mathbf{w}}+\frac{2\zeta}{S}\dot{\hat{\mathbf{w}}}+\frac{2L^4}{S^2}\boldsymbol{\Gamma}_1^{-1}\boldsymbol{\Gamma}_3\hat{\mathbf{w}}-\beta_1\boldsymbol{\Gamma}_1^{-1}\boldsymbol{\Gamma}_2\hat{\mathbf{w}}-\beta_2\boldsymbol{\Gamma}_1^{-1}\boldsymbol{\Gamma}_8\hat{\varphi}\end{aligned}$$

$$+\alpha_1\boldsymbol{\Gamma}_1^{-1}\boldsymbol{\Gamma}_{d3}\left(2\dot{\hat{y}}_1-\hat{\theta}\hat{\varphi}\hat{y}_1-\hat{\theta}^2\hat{z}_1-\hat{z}_1\right)+\alpha_1\boldsymbol{\Gamma}_1^{-1}\boldsymbol{\Gamma}_{d1}\left(2\dot{\hat{\mathbf{v}}}-\hat{\varphi}\hat{\theta}\,\hat{\mathbf{v}}-\hat{\theta}^2\hat{\mathbf{w}}-\hat{\mathbf{w}}\right)$$
$$+\frac{\alpha_2}{2}\boldsymbol{\Gamma}_1^{-1}\boldsymbol{\Gamma}_{d3}\left(2\dot{\hat{\theta}}-2\hat{\varphi}\hat{\theta}^2-\hat{\varphi}\right)-\gamma_1\boldsymbol{\Gamma}_1^{-1}\boldsymbol{\Gamma}_{d2}\hat{\mathbf{w}}-\gamma_2\boldsymbol{\Gamma}_1^{-1}\boldsymbol{\Gamma}_{d4}\hat{\varphi}\big] \tag{A.4}$$

$$\hat{\mathbf{H}}_{y1}=-\frac{1}{\delta}\boldsymbol{\Gamma}_{6-1}^{-1}\boldsymbol{\Gamma}_{6-2}\left(2\dot{\hat{\varphi}}+2\hat{\varphi}^2\hat{\theta}+\hat{\theta}\right)-\boldsymbol{\Gamma}_{6-1}^{-1}\boldsymbol{\Gamma}_9\left(2\dot{\hat{\mathbf{w}}}+\hat{\varphi}\hat{\theta}\,\hat{\mathbf{w}}+\hat{\varphi}^2\hat{\mathbf{v}}+\hat{\mathbf{v}}\right)$$
$$-\left(2\dot{\hat{z}}_1+\hat{\theta}\hat{\varphi}\hat{z}_1+\hat{\varphi}^2\hat{y}_1+\hat{y}_1\right)-\alpha_1\boldsymbol{\Gamma}_{6-1}^{-1}\left(2\dot{\hat{z}}_1+\hat{\theta}\hat{\varphi}\hat{z}_1+\hat{\varphi}^2\hat{y}_1+\hat{y}_1\right)$$
$$-\alpha_1\boldsymbol{\Gamma}_{6-1}^{-1}\boldsymbol{\Gamma}_{d5}\left(2\dot{\hat{\mathbf{w}}}+\hat{\varphi}\hat{\theta}\,\hat{\mathbf{w}}+\hat{\varphi}^2\hat{\mathbf{v}}+\hat{\mathbf{v}}\right)-\frac{\alpha_2}{2}\boldsymbol{\Gamma}_{6-1}^{-1}\left(2\dot{\hat{\varphi}}+2\hat{\varphi}^2\hat{\theta}+\hat{\theta}\right) \tag{A.5}$$
$$+\frac{L\,\boldsymbol{\Gamma}_{6-1}^{-1}}{S_{yy}^2}\hat{y}_1+\left(\frac{L\,\boldsymbol{\Gamma}_{6-1}^{-1}}{S_{yz}^2}+\frac{L\,\boldsymbol{\Gamma}_{6-1}^{-1}}{S_{zy}^2}\right)\hat{z}_1+\frac{L^2\,\boldsymbol{\Gamma}_{6-1}^{-1}}{\delta S_{yy}^2}\hat{\theta}+\frac{L^2\,\boldsymbol{\Gamma}_{6-1}^{-1}}{\delta S_{zy}^2}\hat{\varphi}+\frac{2\xi_{yy}L\,\boldsymbol{\Gamma}_{6-1}^{-1}}{S_{yy}}\dot{\hat{y}}_1$$
$$+\left(\frac{2\xi_{yz}L\,\boldsymbol{\Gamma}_{6-1}^{-1}}{S_{yz}}+\frac{2\xi_{zy}L\,\boldsymbol{\Gamma}_{6-1}^{-1}}{S_{zy}}\right)\dot{\hat{z}}_1+\frac{2\xi_{yy}L^2\,\boldsymbol{\Gamma}_{6-1}^{-1}}{\delta S_{yy}}\dot{\hat{\theta}}+\frac{2\xi_{zy}L^2\,\boldsymbol{\Gamma}_{6-1}^{-1}}{\delta S_{zy}}\dot{\hat{\varphi}}$$

$$\hat{\mathbf{H}}_{\theta}=-\delta^2\boldsymbol{\Gamma}_7^{-1}\boldsymbol{\Gamma}_{6-1}\left(-\hat{\theta}\hat{z}_1^2-\hat{\varphi}\,\hat{y}_1\hat{z}_1\right)-\delta\boldsymbol{\Gamma}_7^{-1}\boldsymbol{\Gamma}_{6-2}\left(2\dot{\hat{z}}_1+4\hat{\theta}\hat{\varphi}\hat{z}_1+2\hat{\varphi}^2\hat{y}_1+\hat{y}_1\right)$$
$$-\delta^2\boldsymbol{\Gamma}_7^{-1}\boldsymbol{\Gamma}_9\left(2\hat{\theta}\hat{z}_1\hat{\mathbf{w}}+\hat{\varphi}\,\hat{y}_1\hat{\mathbf{w}}+\hat{\varphi}\,\hat{z}_1\hat{\mathbf{v}}\right)-\delta\boldsymbol{\Gamma}_7^{-1}\boldsymbol{\Gamma}_{10}\left(2\dot{\hat{\mathbf{w}}}+4\hat{\varphi}\hat{\theta}\,\hat{\mathbf{w}}+2\hat{\varphi}^2\hat{\mathbf{v}}+\hat{\mathbf{v}}\right)$$
$$-\delta^2\boldsymbol{\Gamma}_7^{-1}\left(\hat{\theta}\,\hat{\mathbf{w}}^T\boldsymbol{\Gamma}_1\hat{\mathbf{w}}+\hat{\varphi}\hat{\mathbf{v}}^T\boldsymbol{\Gamma}_1\hat{\mathbf{w}}\right)-\left(2\dot{\hat{\varphi}}+4\hat{\varphi}^2\hat{\theta}+\hat{\theta}\right)-\beta_1\delta\boldsymbol{\Gamma}_7^{-1}\boldsymbol{\Gamma}_{11}\mathbf{v}$$
$$-\beta_1\boldsymbol{\Gamma}_7^{-1}\boldsymbol{\Gamma}_{6-1}\hat{\theta}-\frac{\alpha_3}{2}\boldsymbol{\Gamma}_7^{-1}\left(2\dot{\hat{z}}_1+4\hat{\theta}\hat{\varphi}\hat{z}_1+2\hat{\varphi}^2\hat{y}_1+\hat{y}_1\right)-\frac{\alpha_4}{4}\boldsymbol{\Gamma}_7^{-1}\left(2\dot{\hat{\varphi}}+4\hat{\varphi}^2\hat{\theta}+\hat{\theta}\right) \tag{A.6}$$
$$-\alpha_5\boldsymbol{\Gamma}_7^{-1}\left(\hat{\theta}\hat{z}_1^2+\hat{\varphi}\,\hat{y}_1\hat{z}_1+\hat{\theta}\,\hat{\mathbf{w}}^T\boldsymbol{\Gamma}_{d1}\hat{\mathbf{w}}+\hat{\varphi}\hat{\mathbf{v}}^T\boldsymbol{\Gamma}_{d1}\hat{\mathbf{w}}\right)-\frac{\alpha_3}{2}\boldsymbol{\Gamma}_7^{-1}\boldsymbol{\Gamma}_{d5}\left(2\dot{\hat{\mathbf{w}}}+4\hat{\varphi}\hat{\theta}\,\hat{\mathbf{w}}+2\hat{\varphi}^2\hat{\mathbf{v}}+\hat{\mathbf{v}}\right)$$
$$-\alpha_5\boldsymbol{\Gamma}_7^{-1}\boldsymbol{\Gamma}_{d5}\left(2\hat{\theta}\hat{z}_1\hat{\mathbf{w}}+\hat{\varphi}\,\hat{y}_1\hat{\mathbf{w}}+\hat{\varphi}\,\hat{z}_1\hat{\mathbf{v}}\right)-\gamma_1\boldsymbol{\Gamma}_7^{-1}\hat{\theta}-\gamma_2\delta\boldsymbol{\Gamma}_7^{-1}\hat{\mathbf{v}}+\frac{L^2\delta\boldsymbol{\Gamma}_7^{-1}}{S_{yy}^2}\hat{y}_1+\frac{L^2\delta\boldsymbol{\Gamma}_7^{-1}}{S_{zy}^2}\hat{z}_1$$
$$+\frac{L^3\boldsymbol{\Gamma}_7^{-1}}{S_{yy}^2}\hat{\theta}+\frac{L^3\boldsymbol{\Gamma}_7^{-1}}{S_{zy}^2}\hat{\varphi}+\frac{2\xi_{yy}L^2\delta\boldsymbol{\Gamma}_7^{-1}}{S_{yy}}\dot{\hat{y}}_1+\frac{2\xi_{zy}L^2\delta\boldsymbol{\Gamma}_7^{-1}}{S_{zy}}\dot{\hat{z}}_1+\frac{2\xi_{yy}L^3\boldsymbol{\Gamma}_7^{-1}}{S_{yy}}\dot{\hat{\theta}}+\frac{2\xi_{zy}L^3\boldsymbol{\Gamma}_7^{-1}}{S_{zy}}\dot{\hat{\varphi}}$$

$$\hat{\mathbf{H}}_{z1}=\frac{1}{\delta}\boldsymbol{\Gamma}_{6-1}^{-1}\boldsymbol{\Gamma}_{6-2}\left(2\dot{\hat{\theta}}-2\hat{\theta}^2\hat{\varphi}-\hat{\varphi}\right)+\boldsymbol{\Gamma}_{6-1}^{-1}\boldsymbol{\Gamma}_9\left(2\dot{\hat{\mathbf{v}}}-\hat{\varphi}\hat{\theta}\,\hat{\mathbf{v}}-\hat{\theta}^2\hat{\mathbf{w}}-\hat{\mathbf{w}}\right)$$
$$+\left(2\dot{\hat{y}}_1-\hat{\theta}\hat{\varphi}\hat{y}_1-\hat{\theta}^2\hat{z}_1-\hat{z}_1\right)+\alpha_1\boldsymbol{\Gamma}_{6-1}^{-1}\left(2\dot{\hat{y}}_1-\hat{\theta}\hat{\varphi}\hat{y}_1-\hat{\theta}^2\hat{z}_1-\hat{z}_1\right)$$
$$+\alpha_1\boldsymbol{\Gamma}_{6-1}^{-1}\boldsymbol{\Gamma}_{d5}\left(2\dot{\hat{\mathbf{v}}}-\hat{\varphi}\hat{\theta}\,\hat{\mathbf{v}}-\hat{\theta}^2\hat{\mathbf{w}}-\hat{\mathbf{w}}\right)+\frac{\alpha_2}{2}\boldsymbol{\Gamma}_{6-1}^{-1}\left(2\dot{\hat{\theta}}-2\hat{\theta}^2\hat{\varphi}-\hat{\varphi}\right)+\frac{L\,\boldsymbol{\Gamma}_{6-1}^{-1}}{S_{zz}^2}\hat{z}_1 \tag{A.7}$$
$$+\left(\frac{L\,\boldsymbol{\Gamma}_{6-1}^{-1}}{S_{yz}^2}+\frac{L\,\boldsymbol{\Gamma}_{6-1}^{-1}}{S_{zy}^2}\right)\hat{y}_1+\frac{L^2\,\boldsymbol{\Gamma}_{6-1}^{-1}}{\delta S_{zy}^2}\hat{\theta}+\frac{L^2\,\boldsymbol{\Gamma}_{6-1}^{-1}}{\delta S_{zz}^2}\hat{\varphi}+\frac{2\xi_{zz}L\,\boldsymbol{\Gamma}_{6-1}^{-1}}{S_{zz}}\dot{\hat{z}}_1$$
$$+\left(\frac{2\xi_{yz}L\,\boldsymbol{\Gamma}_{6-1}^{-1}}{S_{yz}}+\frac{2\xi_{zy}L\,\boldsymbol{\Gamma}_{6-1}^{-1}}{S_{zy}}\right)\dot{\hat{y}}_1+\frac{2\xi_{zy}L^2\,\boldsymbol{\Gamma}_{6-1}^{-1}}{\delta S_{zy}}\dot{\hat{\theta}}+\frac{2\xi_{zz}L^2\,\boldsymbol{\Gamma}_{6-1}^{-1}}{\delta S_{zz}}\dot{\hat{\varphi}}$$

© VIBROENGINEERING. JOURNAL OF VIBROENGINEERING. JUNE 2012. VOLUME 14, ISSUE 2. ISSN 1392-8716

$$\hat{\mathbf{H}}_{\varphi} = -\delta^2\boldsymbol{\Gamma}_7^{-1}\boldsymbol{\Gamma}_{6-1}\left(\hat{\varphi}\,\hat{y}_1^2 + \hat{\theta}\,\hat{y}_1\hat{z}_1\right) + \delta\boldsymbol{\Gamma}_7^{-1}\boldsymbol{\Gamma}_{6-2}\left(2\dot{\hat{y}}_1 - 4\hat{\theta}\hat{\varphi}\hat{y}_1 - 2\hat{\theta}^2\hat{z}_1 - \hat{z}_1\right)$$
$$-\delta^2\boldsymbol{\Gamma}_7^{-1}\boldsymbol{\Gamma}_9\left(2\hat{\varphi}\,\hat{y}_1\hat{\mathbf{v}} + \hat{\theta}\,\hat{y}_1\hat{\mathbf{w}} + \hat{\theta}\,\hat{z}_1\hat{\mathbf{v}}\right) + \delta\boldsymbol{\Gamma}_7^{-1}\boldsymbol{\Gamma}_{10}\left(2\dot{\hat{\mathbf{v}}} - 4\hat{\varphi}\hat{\theta}\,\hat{\mathbf{v}} - 2\hat{\theta}^2\hat{\mathbf{w}} - \hat{\mathbf{w}}\right)$$
$$-\delta^2\boldsymbol{\Gamma}_7^{-1}\left(\hat{\theta}\,\hat{\mathbf{w}}^T\boldsymbol{\Gamma}_1\hat{\mathbf{v}} + \hat{\varphi}\hat{\mathbf{v}}^T\boldsymbol{\Gamma}_1\hat{\mathbf{v}}\right) + \left(2\dot{\hat{\theta}} - 4\hat{\theta}^2\hat{\varphi} - \hat{\varphi}\right) - \beta_1\delta\boldsymbol{\Gamma}_7^{-1}\boldsymbol{\Gamma}_{11}\hat{\mathbf{w}}$$
$$-\beta_1\boldsymbol{\Gamma}_7^{-1}\boldsymbol{\Gamma}_{6-1}\hat{\varphi} + \frac{\alpha_3}{2}\boldsymbol{\Gamma}_7^{-1}\left(2\dot{\hat{y}}_1 - 4\hat{\theta}\hat{\varphi}\hat{y}_1 - 2\hat{\theta}^2\hat{z}_1 - \hat{z}_1\right) + \frac{\alpha_4}{4}\boldsymbol{\Gamma}_7^{-1}\left(2\dot{\hat{\theta}} - 4\hat{\theta}^2\hat{\varphi} - \hat{\varphi}\right)$$
$$-\alpha_5\boldsymbol{\Gamma}_7^{-1}\left(\hat{\varphi}\,\hat{y}_1^2 + \hat{\theta}\,\hat{y}_1\hat{z}_1 + \hat{\theta}\,\hat{\mathbf{w}}^T\boldsymbol{\Gamma}_{d1}\hat{\mathbf{v}} + \hat{\varphi}\hat{\mathbf{v}}^T\boldsymbol{\Gamma}_{d1}\hat{\mathbf{v}}\right) \tag{A.8}$$
$$+\frac{\alpha_3}{2}\boldsymbol{\Gamma}_7^{-1}\boldsymbol{\Gamma}_{d5}\left(2\dot{\hat{\mathbf{v}}} - 4\hat{\varphi}\hat{\theta}\,\hat{\mathbf{v}} - 2\hat{\theta}^2\hat{\mathbf{w}} - \hat{\mathbf{w}}\right) - \alpha_5\boldsymbol{\Gamma}_7^{-1}\boldsymbol{\Gamma}_{d5}\left(\hat{\theta}\hat{z}_1\hat{\mathbf{v}} + \hat{\theta}\,\hat{y}_1\hat{\mathbf{w}} + 2\hat{\varphi}\,\hat{y}_1\hat{\mathbf{v}}\right)$$
$$-\gamma_1\boldsymbol{\Gamma}_7^{-1}\hat{\varphi} - \gamma_2\delta\boldsymbol{\Gamma}_7^{-1}\boldsymbol{\Gamma}_{d6}\hat{\mathbf{w}} + \frac{L^2\delta\boldsymbol{\Gamma}_7^{-1}}{S_{zz}^2}\hat{z}_1 + \frac{L^2\delta\boldsymbol{\Gamma}_7^{-1}}{S_{zy}^2}\hat{y}_1 + \frac{L^3\boldsymbol{\Gamma}_7^{-1}}{S_{zz}^2}\hat{\varphi} + \frac{L^3\boldsymbol{\Gamma}_7^{-1}}{S_{zy}^2}\hat{\theta}$$
$$+\frac{2\xi_{zz}L^2\delta\boldsymbol{\Gamma}_7^{-1}}{S_{zz}}\dot{\hat{z}}_1 + \frac{2\xi_{zy}L^2\delta\boldsymbol{\Gamma}_7^{-1}}{S_{zy}}\dot{\hat{y}}_1 + \frac{2\xi_{zz}L^3\boldsymbol{\Gamma}_7^{-1}}{S_{zz}}\dot{\hat{\varphi}} + \frac{2\xi_{zy}L^3\boldsymbol{\Gamma}_7^{-1}}{S_{zy}}\dot{\hat{\theta}}$$

Appendix B

$$\boldsymbol{\Gamma}_1 = \int_0^L (\boldsymbol{\Psi}(x)\boldsymbol{\Psi}^T(x))dx \quad \text{(B.1)} \qquad \boldsymbol{\Gamma}_2 = \int_0^L (\boldsymbol{\Psi}'(x)\boldsymbol{\Psi}'^T(x))dx \quad \text{(B.2)}$$

$$\boldsymbol{\Gamma}_3 = \int_0^L (\boldsymbol{\Psi}''(x)\boldsymbol{\Psi}''^T(x))dx \quad \text{(B.3)} \qquad \boldsymbol{\Gamma}_4 = \int_0^L (x\,\boldsymbol{\Psi}(x))dx \quad \text{(B.4)}$$

$$\boldsymbol{\Gamma}_5 = \int_0^L (\boldsymbol{\Psi}(x))dx \quad \text{(B.5)} \qquad \boldsymbol{\Gamma}_{6-1} = \int_0^L dx \quad \text{(B.6)}$$

$$\boldsymbol{\Gamma}_{6-2} = \int_0^L x\,dx \quad \text{(B.7)} \qquad \boldsymbol{\Gamma}_7 = \int_0^L x^2 dx \quad \text{(B.8)}$$

$$\boldsymbol{\Gamma}_8 = \int_0^L (\boldsymbol{\Psi}'(x))dx \quad \text{(B.9)} \qquad \boldsymbol{\Gamma}_9 = \int_0^L (\boldsymbol{\Psi}^T(x))dx \quad \text{(B.10)}$$

$$\boldsymbol{\Gamma}_{10} = \int_0^L (x\,\boldsymbol{\Psi}^T(x))dx \quad \text{(B.11)} \qquad \boldsymbol{\Gamma}_{11} = \int_0^L (\boldsymbol{\Psi}'^T(x))dx \quad \text{(B.12)}$$

$$\boldsymbol{\Gamma}_{d1} = \boldsymbol{\Psi}(x = L/2)\boldsymbol{\Psi}^T(x = L/2) \quad \text{(B.13)} \qquad \boldsymbol{\Gamma}_{d2} = \boldsymbol{\Psi}'(x = L/2)\boldsymbol{\Psi}'^T(x = L/2) \quad \text{(B.14)}$$

$$\boldsymbol{\Gamma}_{d3} = \boldsymbol{\Psi}(x = L/2) \quad \text{(B.15)} \qquad \boldsymbol{\Gamma}_{d4} = \boldsymbol{\Psi}'(x = L/2) \quad \text{(B.16)}$$

$$\boldsymbol{\Gamma}_{d5} = \boldsymbol{\Psi}^T(x = L/2) \quad \text{(B.17)} \qquad \boldsymbol{\Gamma}_{d6} = \boldsymbol{\Psi}'^T(x = L/2) \quad \text{(B.18)}$$

References

[1] **Huang H.-Y., Schlack A. L., Jr.** Lyapunov stability analysis of elastic shaft-rigid disk-bearing systems. Journal of Applied Mechanics, Vol. 59, 1992, p. 946–954.

[2] **Rao J. S., Shiau T. N., Chang J. R.** Theoretical analysis of lateral response due to torsional excitation of geared rotors. Mechanism and Machine Theory, Vol. 33, 1998, p. 761–783.

[3] **El-Marhomy A. A.** Dynamics and stability of elastic shaft-bearing systems with nonlinear bearing parameters. Heat and Mass Transfer, Vol. 35, 1999, p. 334–344.

[4] **Z. Ji, J. W. Zu** Method of multiple scales for vibration analysis of rotor shaft systems with nonlinear bearing pedestal model. Journal of Sound and Vibration, Vol. 218, 1998, p. 293–305.

[5] **El-Marhomy A. A., Abdel-Sattar N. E.** Stability analysis of rotor-bearing systems via Routh-Hurwitz criterion. Applied Energy, Vol. 77, 2004, p. 287–308.

[6] **Mourelatos K., Hu Z. P., Vlahopoulos N.** Computational analysis for dynamic response of a rotating shaft on flexible support structure with clearances. Journal of Sound and Vibration, Vol. 267, 2003, p. 1–28.

[7] **Jia-Jang Wu** Prediction of lateral vibration characteristics of a full-size rotor-bearing system by using those of its scale models. Finite Elements in Analysis and Design, Vol. 43, 2007, p. 803–816.

[8] **Ishida Y., Inagaki M., Ejima R., Hayashi A.** Nonlinear resonances and self-excited oscillations of a rotor caused by radial clearance and collision. Nonlinear Dynamics, Vol. 57, 2009, p. 593–605.

[9] **Meruane V., Pascual R.** Identification of nonlinear dynamic coefficients in plain journal bearings. Tribology International, Vol. 41, 2008, p. 743–754.

[10] **Baguet S., Jacquenot G.** Nonlinear couplings in a gear-shaft-bearing system. Mechanism and Machine Theory, Vol. 45, 2010, p. 1777–1796.

[11] **Va´zquez Jose´ A., Barrett Lloyd E., Flack Ronald D.** A flexible rotor on flexible bearing supports: stability and unbalance response. Journal of Vibration and Acoustics, Vol. 123, 2001, p. 137–144.

[12] **Lin Jaw-Ren** Linear stability analysis of rotor-bearing system: couple stress fluid model. Computers and Structures, Vol. 79, 2001, p. 801–809.

[13] **Legrand M., Jiang D., Pierre C., Shaw S. W.** Nonlinear normal modes of a rotating shaft based on the invariant manifold method. International Journal of Rotating Machinery, Vol. 10, 2004, p. 319–335.

[14] **Chang-Jian Cai-Wan** Nonlinear numerical analysis of a flexible rotor equipped with squeeze couple stress fluid film journal bearings. Acta Mechanica Solida Sinica, Vol. 20, 2007, p. 309–316.

[15] **Chang-Jian Cai-Wan, Cha'o-Kuang Chen** Couple stress fluid improve rub-impact rotor-bearing system – Nonlinear dynamic analysis. Applied Mathematical Modeling, Vol. 34, 2010, p. 1763–1778.

[16] **Jawaid I. Inayat-Hussain** Bifurcations in the response of a flexible rotor in squeeze-film dampers with retainer springs. Chaos, Solitons and Fractals, Vol. 39, 2009, p. 519–532.

[17] **Chang-Jian Cai-Wan, Kuo Jenn-Kun** Bifurcation and chaos for porous squeeze film damper mounted rotor–bearing system lubricated with micro polar fluid. Nonlinear Dynamics, Vol. 58, 2009, p. 697–714.

[18] **Das A. S., Dutt J. K., Ray K.** Active vibration control of unbalanced flexible rotor–shaft systems parametrically excited due to base motion. Applied Mathematical Modeling, Vol. 34, 2010, p. 2353–2369.

[19] **Chang-Jian Cai-Wan, Her-Terng Yau, Jiann-Lin Chen** Nonlinear dynamic analysis of a hybrid squeeze-film damper-mounted rigid rotor lubricated with couple stress fluid and active control. Applied Mathematical Modeling, Vol. 34, 2010, p. 2493–2507.

[20] **Khanlo H. M., Ghayour M., Ziaei-Rad S.** Chaotic vibration analysis of rotating flexible continuous shaft-disk system with a rub-impact between the disk and the stator. Commun. Nonlinear Sci. Numer. Simulat., Vol. 16, 2011, p. 566–582.

[21] **Meirovitch L.** Principles and Techniques of Vibrations, Prentice-Hall Inc., 1997.

[22] **Abdul Azeez M. F., Vakakis A. F.** Numerical and experimental analysis of a continuous overhung rotor undergoing vibro-impact. International Journal of Non-linear Mechanics, Vol. 34, 1999, p. 415–435.

[23] **Lee H. P.** Dynamic response of a rotating Timoshenko shaft subject to axial forces and moving loads. Journal of Sound and Vibration, Vol. 181, 1995, p. 169–177.

[24] **Nayfeh A. H., Balachandran B.** Applied Nonlinear Dynamics. John Wiley and Sons Inc., 1995.

[25] **Jianxue Xu** Some advances on global analysis of nonlinear systems. Chaos, Solitons and Fractals, Vol. 39, 2009, p. 1839–1848.

[26] **Wolf A., Swift J. B., Swinney H. L., Vastano J. A.** Determining Lyapunov exponents from a time series. Physica D, Vol. 16, 1985, p. 285–317.

© VIBROENGINEERING. JOURNAL OF VIBROENGINEERING. JUNE 2012. VOLUME 14, ISSUE 2. ISSN 1392-8716